AD-A255 093

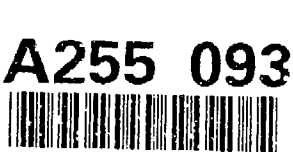

(2)

NSWC TR 89-212

IGNITION OF PBXW-115 DUE TO ELECTROSTATIC DISCHARGE

BY RICHARD J. LEE, DOUGLAS G. TASKER,
JERRY W. FORBES, and BRUCE C. BEARD

RESEARCH AND TECHNOLOGY DEPARTMENT

MAY 1991

DTIC
ELECTE
SEP 04 1992
S A D

Approved for public release; distribution is unlimited.

NAVAL SURFACE WARFARE CENTER

Dahlgren, Virginia 22448-5000 • Silver Spring, Maryland 20903-5000

92 9 02 058

418546 92-24350

5918.

IGNITION OF PBXW-115 DUE TO ELECTROSTATIC DISCHARGE

BY RICHARD J. LEE, DOUGLAS G. TASKER,
JERRY W. FORBES, and BRUCE C. BEARD

RESEARCH AND TECHNOLOGY DEPARTMENT

MAY 1991

Accesion For
NTIS CRA&I
DTIC TAB
Unannounced
Justification
By
Distribution /
Availability Codes
Dist | Avail and / or Special
A-1

Approved for public release; distribution is unlimited.

DTIC QUALITY INSPECTED 1

NAVAL SURFACE WARFARE CENTER
Dahlgren, Virginia 22448-5000 • Silver Spring, Maryland 20903-5000

FOREWORD

Naval munitions, especially those contained in insulating cases, are at risk due to electrostatic discharge (ESD) yet existing Navy test procedures do not adequately determine these risks. Electric energy can be stored on such cases through electrostatic charging as a result of normal handling or thermal cycling. The stored energies (from 30 mJ to many J) are comparable to those observed for ignition in propellants with similar compositions to Naval PBX explosives.

Present ESD test methods do not allow for the effects of confinement or the rate of electric energy deposition. Recent studies have indicated that an increase in confinement reduces the critical energy for ESD ignition by several orders of magnitude.

Before the ESD problem can be resolved, the following four items need to be addressed: (1) the electric energy transfer associated with insulated cases, (2) the effect of the discharge profile on the reaction sensitivity, (3) the effect of confinement on the sensitivity and (4) an ignition mechanism for explosives. This report offers data for the latter three.

Data from capacitive discharge experiments on an aluminized explosive, PBXW-115, suggest that the power profile and confinement are important to ESD ignition sensitivity. Based on our observations, a model describing the shock ignition of a solid explosive has been developed.

This work was funded by the Office Of Naval Technology as part of the NSWC Explosives and Undersea Warheads Block Program.

We thank M. Cowperthwaite of SRI International and B. Hammant of Ministry of Defense, U.K., for their helpful comments on this work. We are indebted to B. Snowden, N. Snowden and R. Hay for their fine experimental work.

Authorized by:

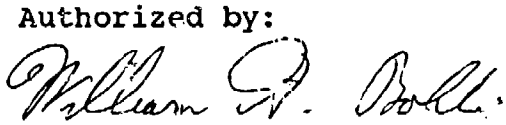

WILLIAM H. BOHLI, Acting Head
Explosives Division

CONTENTS

Chapter		Page
1	INTRODUCTION	1-1
2	CAPACITIVE DISCHARGE EXPERIMENTS	2-1
	TEST CELL	2-1
	TEST CIRCUIT AND DIAGNOSTICS	2-3
	ROGOWSKI COIL	2-3
	CURRENT PROBE	2-5
	VOLTAGE PROBE	2-7
3	X-RAY PHOTOELECTRON SPECTROSCOPY (XPS) STUDIES	3-1
	XPS, THE TECHNIQUE	3-1
	SAMPLE PREPARATION AND ANALYSIS	3-2
4	PRE-BREAKDOWN CONDUCTION	4-1
	PRE-BREAKDOWN CURRENT	4-1
	SERIES CIRCUIT RESISTANCE	4-5
	CAPACITANCE	4-5
	VOLTAGE	4-5
	VARIATION IN ACTIVE AREA	4-7
	IGNITION PRIOR TO BREAKDOWN	4-7
5	IGNITION RESULTS	5-1
	EFFECT OF RESTRAINT	5-1
	XPS RESULTS	5-1
	XPS SPECTRA FROM CONTROL SAMPLES	5-1
	XPS SPECTRA FROM DISCHARGED SAMPLES	5-5
	SUMMARY	5-8
	PHYSICAL NATURE OF DISCHARGE CHANNELS	5-8
	ENERGY AND POWER	5-8
6	SHOCK IGNITION THEORY	6-1
	REACTION THRESHOLD DEFINITIONS	6-1
	APPLICATIONS TO ESD	6-1
	THEORY	6-2
	SHOCK PRESSURE	6-2
	SHOCK VELOCITY	6-3
	SHOCK PULSE WIDTH	6-3
	ENERGY FLUENCE	6-6
	EFFECT OF POWER AND ARC DYNAMICS	6-6

CONTENTS (Cont.)

Chapter		Page
7	DISCUSSION	7-1
	TEST METHODS	7-1
	POWER PROFILE	7-1
	CONFINEMENT	7-2
	PRESENT THEORY	7-2
	FUTURE WORK	7-3
8	CONCLUSIONS	8-1
	REFERENCES	9-1

ILLUSTRATIONS

Figure		Page
2-1	TEST CELL	2-2
2-2	TEST CIRCUIT	2-4
2-3	ROGOWSKI COIL	2-4
2-4	CURRENT PROBE	2-6
2-5	VOLTAGE PROBE	2-8
4-1	CURRENT AND VOLTAGE ILLUSTRATION FOR TYPICAL EXPERIMENT	4-2
4-2	PRE-BREAKDOWN CURRENT	4-4
4-3	VOLTAGE AND CURRENT FOR SAMPLE 9, 400 nF AT 9 kV	4-6
4-4	ACTIVE ANODE DIAMETER vs ENERGY TO BREAKDOWN	4-8
5-1	PHYSICAL RESULTS OF DISCHARGE EXPERIMENTS	5-3
5-2	NITROGEN SPECTRA FOR AP, HMX AND PBXW-115	5-4
5-3	NITROGEN SPECTRA FOR SAMPLES 3 AND 14	5-6
5-4	CHLORINE SPECTRA FOR SAMPLES 3 AND 14	5-7
5-5	CROSS SECTION OF ARC CHANNELS FROM SAMPLE 11	5-9
5-6	CROSS SECTION OF ARC CHANNELS FROM SAMPLE 9	5-9
6-1	SIMPLE HYDRODYNAMICS OF A THERMALLY EXPLODED ARC CHANNEL	6-4

TABLES

Table		Page
4-1	PRE-BREAKDOWN RESULTS	4-3
5-1	POST-BREAKDOWN RESULTS	5-2

CHAPTER 1

INTRODUCTION

Electrostatic discharge (ESD) has been recognized as the cause of several accidental ignitions in large propellant systems.[1,2] The fear is that Naval munitions, especially those contained in insulating cases, are at risk due to ESD, yet existing Navy test procedures do not adequately determine these risks. Present test methods do not allow for the effects of confinement or the rate of electrical energy deposition.

Electric energy can be stored on munition cases through electrostatic charging as a result of normal handling or thermal cycling. Hodges[3] has demonstrated that the electrostatic charge density on the surface of a composite case can be as large as 20 $\mu C/m^2$. Hence the stored energies (from 30 mJ to many J) are comparable to those observed for ignition in propellants with similar compositions to Naval PBX explosives.

Before the ESD problem can be resolved, the following four items must be addressed: (1) the electric energy transfer associated with insulated cases, (2) the effect of the discharge profile on the reaction sensitivity, (3) the effect of confinement on the sensitivity and (4) an ignition mechanism for explosives. This report offers data for the latter three.

In this study, PBXW-115 was found to conduct at electric field strengths exceeding ≈500 kV/m. An energy density of ≈8 x 10^6 J/m^3 was required to induce catastrophic breakdown. Low energy experiments, 3 to 13 Joules deposited to the sample, showed that the energy deposited prior to breakdown was not responsible for ignition.

X-Ray Photoelectron Spectroscopy (XPS) studies confirmed that thermal reaction was confined to the discharge channel. The highly localized energy deposition in an arc channel likely raises the local temperature above that required for thermal ignition. However, a sustained reaction was not observed unless the sample was restrained. This suggests that containment is important for ESD ignition.

A simple analytical model, which is discussed in Chapter 6, has demonstrated that if ESD induces a thermal explosion in an arc channel, then the reaction can be carried to the surrounding mass of unreacted explosive. The analysis given here has shown

that the thermal explosion of a 1 mm diameter cylinder of PBXW-115 appears to be sufficient to induce *first reaction*, i.e., a rapid deflagration that is too weak to accelerate to detonation.

CHAPTER 2

CAPACITIVE DISCHARGE EXPERIMENTS

A capacitive discharge circuit was used to deposit electrical energy in an aluminized explosive, PBXW-115. Voltage, V, current, I, and rate of change of current, dI/dt, data were recorded on 2090 series Nicolet* digital oscilloscopes with a band width of 50 MHz. These data were used to make accurate calculations of the electrical power profile and the energy deposited in the test cell. The deposition energy varied from 3 to 150 J.

These experiments were performed to study pre-breakdown conduction, the energy required for catastrophic dielectric breakdown and ignition. The results for the pre-breakdown conduction and the energy to breakdown are given in Chapter 4. The observations of ignition are described in Chapter 5.

TEST CELL

Cylindrical discs of PBXW-115, 44.45 mm diameter, 6.35 mm thick, were tested between 19.05 mm diameter brass electrodes and mounted in a plastic test cell shown in Figure 2-1. The low voltage electrode was gently pressed against the bottom of the sample to ensure good electrical contacts. The two halves were pushed into a 50.8 mm OD, 47.63 mm ID, 28.58 mm long polymethyl methacrylate (PMMA) tube which held the test cell together. Retaining bolts were used to restrain test samples. Experiments were also performed without the retaining bolts.

The Teflon end-caps formed a convoluted path between the high voltage and ground electrode inside and outside the test cell to suppress surface flash-over. Surface flash-over around the sample was suppressed by applying silicone rubber encapsulant RTV 3145 Gray† around the sample's periphery, thereby gluing the sample to the inside ledge of the test cell.

---

* Nicolet Instrument Corporation, Test Instrument Division, 4720-F Boston Way, Lanham, MD.

† RTV 3145, Dow Corning Corporation, Midland, MI 48640.

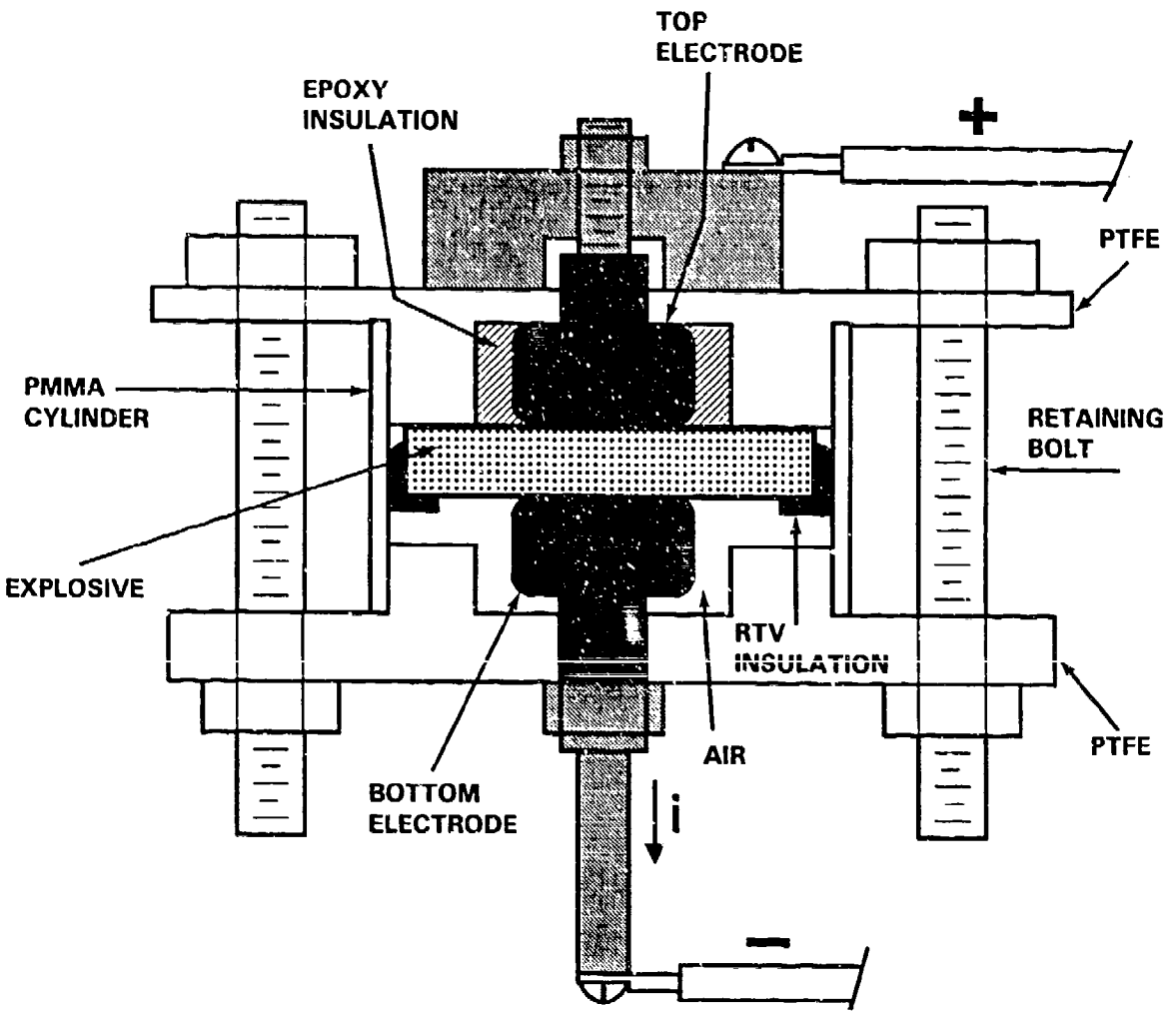

FIGURE 2-1. TEST CELL

Care was taken to ensure that the discharge occurred towards the center of the test sample. The electrodes employed a 3.2 mm (1/8 inch) radius at the edges in order to decrease the divergent field in that region. An epoxy ring, Epon 815* with an Ancamine T1 hardener,† was cast around the cathode to minimize field enhancement at the electrode edges due to dielectric mismatch.[4] A 2.5 mil thick, adhesive backed polyimide insulated tape (Kapton K250 tape)‡ was used to mask over the electrode edges. The spongy PBXW-115 filled this gap under the slight pressure applied by the electrodes. The active area defined by the hole in the Kapton was varied (diameters of 11.5 mm, 4.6 mm and 1.1 mm) to determine if pre-breakdown conduction was localized.

TEST CIRCUIT AND DIAGNOSTICS

The test circuit, shown in Figure 2-2, used one of two capacitances (0.4 μF or 54 μF). The electrical energy was transferred to the sample via a triggered spark gap and 3 m of Reynolds Type C coaxial cable. The 54 μF capacitance charged to 5 kV nominally delivered 150 J to the sample. This capacitance was initially selected because it was available in the discharge circuit at the time. The results from these high energy experiments provided information concerning ESD ignition. Later experiments used a 0.4 μF capacitance charged between 5 and 9 kV to deliver energies of 3 to 13 J. These relatively low energy experiments were performed to study pre-breakdown conduction.

Note that the electrical energy (150 J) delivered to the sample in the ignition experiments is 22 percent of the energy stored in the capacitance (675 J). Note that our circuit efficiency is better than conventional ESD test circuits,[5] which typically have efficiencies less than 10 percent. The low circuit efficiency is attributed to the resistance of the discharge arc being smaller than the circuit impedance.

Rogowski Coil

A Rogowski coil,[5,6,7] shown in Figure 2-3, was placed around an extension of the low voltage electrode to measure the current change, dI/dt, through the sample. The dI/dt data were used to

---

* Epon 815 Resin, Miller Stephenson Chemical Co., Inc., P.O. Box 950, Dandury, CT 06813.

† Ancamine T-1 Hardener, Pacific Anchor Chemical Corporation, 6055 East Washington Blvd, Suite 700, Los Angeles, CA 90040.

‡ Kapton K250 Tape, CHR Industries, Inc., 407 East Street, New Haven, CT 06509.

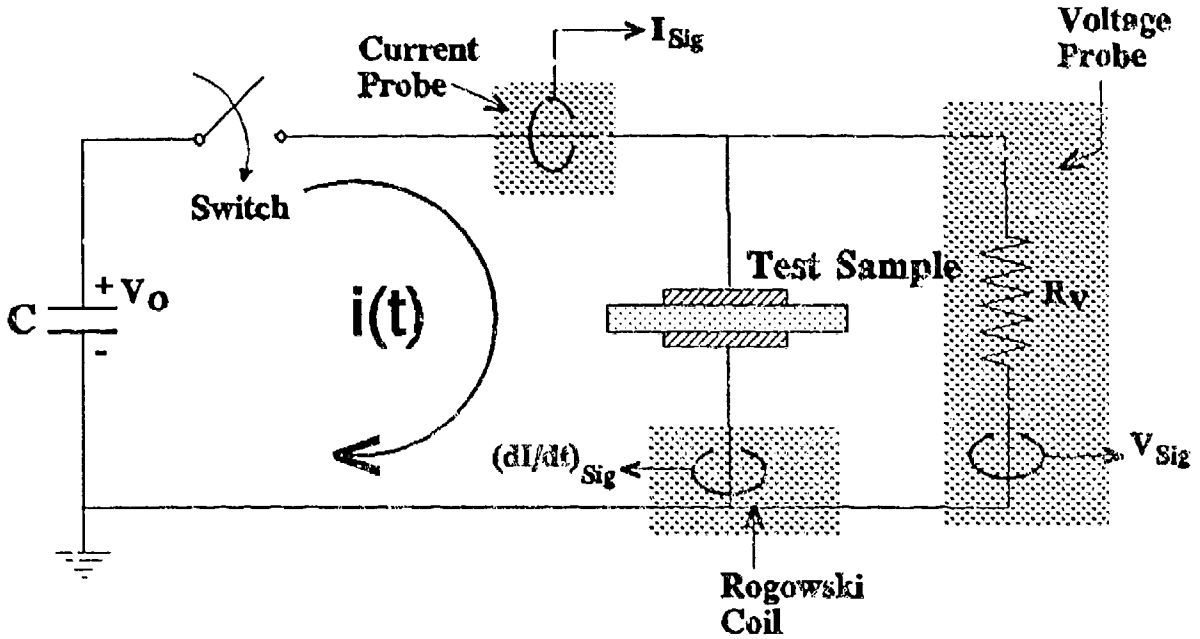

FIGURE 2-2. TEST CIRCUIT

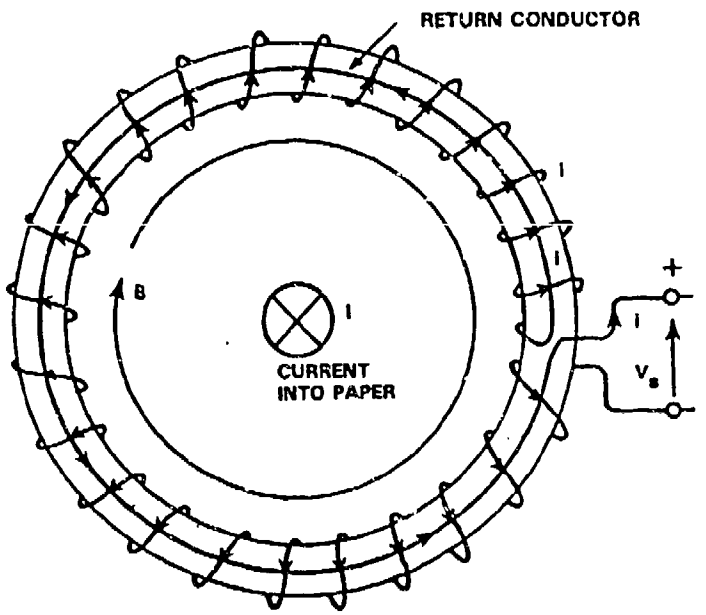

FIGURE 2-3. ROGOWSKI COIL

compensate for L dI/dt, the difference between the true and the measured voltage across the test cell. This difference is due to the rate of change of magnetic flux in the test cell.

The probe had a sensitivity of 1 (GA/s)/volt and a rise time of < 1 ns. The coil was constructed by wrapping a copper ribbon (127 μm (5 mil) thick, 1 mm wide) around a RG-223 cable core. The coil pitch was 1 turn every 5 mm over a 70 mm length which included a 50 Ω metal film resistor at the end (Corning type RN55E, 1/8 Watt, 1%). A plastic shrinkable tubing was used to build up the resistor diameter to match the RG-223 core diameter. The resistor was required to suppress any high frequency ringing.

The voltage signal, V_s, across the coil is a measure of dI/dt associated with the current passing through the center of the loop.

$$V_s(t) = -\mu A N_l \frac{dI}{dt} \qquad (2\text{-}1)$$

where μ is the permeability, N_l is the pitch (number of turns per unit length) and A is the area encompassed by one turn. The signal is halved by the voltage divider created by the 50 Ω resistor and the 50 Ω cable impedance. Therefore the probe's sensitivity is given by:

$$Probe\ Sensitivity = \frac{2}{M} \left(\frac{amps/sec}{volt}\right) \qquad (2\text{-}2)$$

where $M = \mu N_l A$ is the mutual inductance. The coil's self inductance, L, can be estimated by L = N(M) where N is the number of turns in the coil. The self inductance of the Rogowski coil used in this study was 28 nH.

Current Probe

The total current was measured with a Pearson Model 110A* (0.1 volts/amp) current transformer placed along the transmission line. The current probe, shown in Figure 2-4 uses a grounded enclosure to suppress capacitive signal pickup. The combined load resistance (8.33 Ω) of a X10 attenuator and five 10 Ω terminators divided the transformer's output signal by 7. This kept the signal output from exceeding the operational range of the attenuator (1 kV across the output terminal). The overall sensitivity of the probe was nominally 700 amps/volt, including the sensitivity of the basic coil, the effect of the 8.33 Ω loading and the X10 attenuator.

---

* Pearson Electronics, Inc., 1860 Embarcadero Rd, Palo Alto, CA 94303.

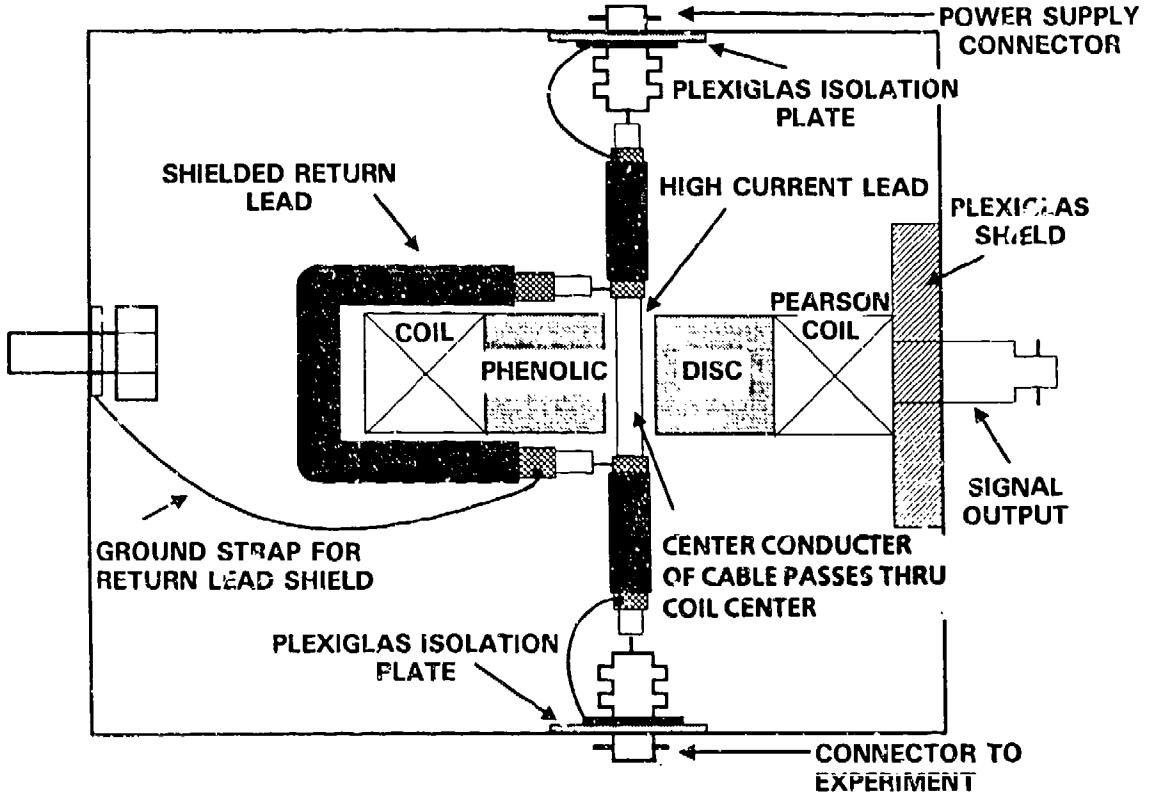

FIGURE 2-4. CURRENT PROBE

Voltage Probe

A copper sulphate voltage probe,[5,6] shown in Figure 2-5, was used directly across the test cell. The copper sulphate resistance was nominally 100 Ω, several orders of magnitude above the arc channel resistance. The current through the resistor was monitored by Pearson probes to eliminate ground loops. Pearson Model 411 (0.1 volt/amp) probes were used so the sensitivity was nominally 1 kV/volt. The Pearson probes and the resistor were housed in separate shielded compartments to suppress capacitive signal pickup.

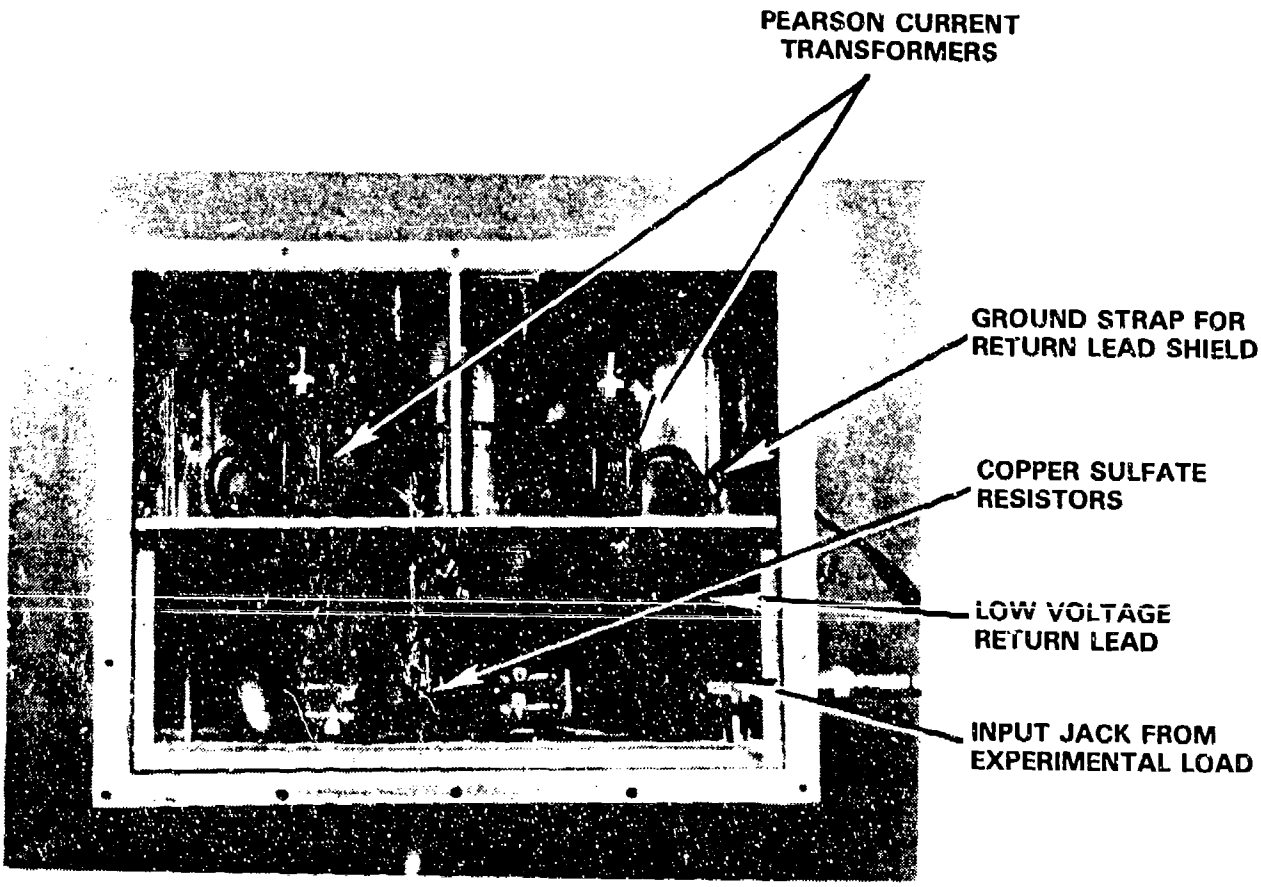

FIGURE 2-5. VOLTAGE PROBE

CHAPTER 3

X-RAY PHOTOELECTRON SPECTROSCOPY (XPS) STUDIES

XPS studies were used to determine the degree of reaction for recovered samples. XPS[8] provides elemental and chemical characterization of material surfaces. The data can also provide an estimation of the quantity of each chemical state present at the surface expressed as a surface atom percentage.

A Physical Electronics 5400 photoelectron spectrometer was used to perform the XPS in this study. Special features incorporated into this instrument include multiple photon sources (dual Mg K_α - Al K_α, monochromatic Al K_α, and He UV resonance lamp), sample cooling and spatially defining electron optics that permit the analysis of features down to 200 μm diameter.

Samples included control materials, i.e., samples that did not undergo electrical discharge testing, of PBXW-115 explosive as well as RDX and AP. Comparisons of spectra from the discharged regions of the recovered samples with those of the control samples clearly demonstrated the chemical changes that occur due to ESD.

XPS, THE TECHNIQUE

XPS is an analytical technique based upon the physics of the photoelectric effect. Absorption of characteristic X-ray photons causes core level ionization, by the emission of electrons from the material. The emitted electrons are then collected and analyzed with respect to their emitted (kinetic) energy. The measured kinetic energy is the difference between the photon energy and the energy required of the electron to escape the attractive forces (binding energy) of the atom. Peaks characteristic of each element appear at well known binding energies in the electron energy spectrum. Shifts in the energy position of these peaks indicate the specific oxidation state and/or bonding environment of the element. Magnesium K_α x-ray photons (1254.6 eV) were used for the spectra collected in this study.

XPS is highly surface specific owing to the limited inelastic path length of the low energy electrons (<1254.6 eV) through material. As a result, analysis depths are typically on

the order of 50 Å. Since the electrons are readily scattered by matter, the analysis must be performed under ultrahigh vacuum to elimina e scattering of the emitted electrons.

In summary, XPS provides elemental and chemical characterization of material surfaces. The data can also provide an estimation of the quantity (expressed as a surface atom percentage) of each chemical state present at the surface.

SAMPLE PREPARATION AND ANALYSIS

All sample manipulation was performed with the greatest care to maintain the nature of the sample surface. Gloves were worn at all times during the cutting and mounting of the samples. The implements used in the cutting and handling of the samples were thoroughly cleaned with ethyl alcohol and acetone prior to each use. Arc channels were accessed for analysis by making radial cuts to the channel. A thin slice of the material containing the arc channel was removed from the resulting wedge. The samples were held onto the mount by double sided tape or by screws.

Samples were cooled to <-30°C under high vacuum in the introduction chamber of the XPS spectrometer. The temperature was maintained within the analysis chamber during the entire period of data acquisition. At the decreased temperature, the vapor pressure was low enough not to corrupt the ultra-high vacuum of the analysis chamber.

CHAPTER 4

PRE-BREAKDOWN CONDUCTION

Electrical conduction prior to dielectric breakdown was observed in PBXW-115 above 0.5 kV/mm. The pre-breakdown phase and subsequent discharge phase are illustrated in Figure 4-1. Each phase can be characterized by the relative magnitude of the voltage. The voltage prior to breakdown is close to the charging voltage across the capacitor. The difference between these two voltages was determined by the pulse impedance of the circuit and the resistance of the sample. The pre-breakdown current was on the order of 100 A. During catastrophic breakdown, the voltage drops sharply and the current increases. The energy remaining in the capacitor (54 μF or 400 nF) following breakdown determined the relative magnitude of the discharge current ($\approx$10 kA or $\approx$1 kA respectively).

It was observed that energies up to 5.5 Joules were necessary before an arc discharge could be formed. This energy to breakdown decreased with decreasing electrode active area, i.e., the electrode area directly in contact with the sample. These results indicate that the pre-breakdown conduction is not localized and consequently does not contribute significantly to ignition.

Table 4-1 displays data pertaining to the pre-breakdown phase of each experiment. Samples 1 and 2 are not displayed in this table because definitive pre-breakdown currents were not obtained for these samples.

Samples 1 through 7 were tested with a 54 μF capacitance at a charging voltage of 5 kV. A series resistance was used to limit the current in samples 6 and 7 in order to observe the effect this would have on the energy to breakdown. Samples 8 through 14 were tested with a 400 nF capacitance at charging voltages ranging from 5 kV to 9.9 kV. The active area of the anode was varied for samples 11 through 14.

PRE-BREAKDOWN CURRENT

Figure 4-2 shows a typical pre-breakdown current profile. The current rose to several hundred amperes within 2 μs and then diminished to a value between 40 and 60 percent of the peak within 6 μs.

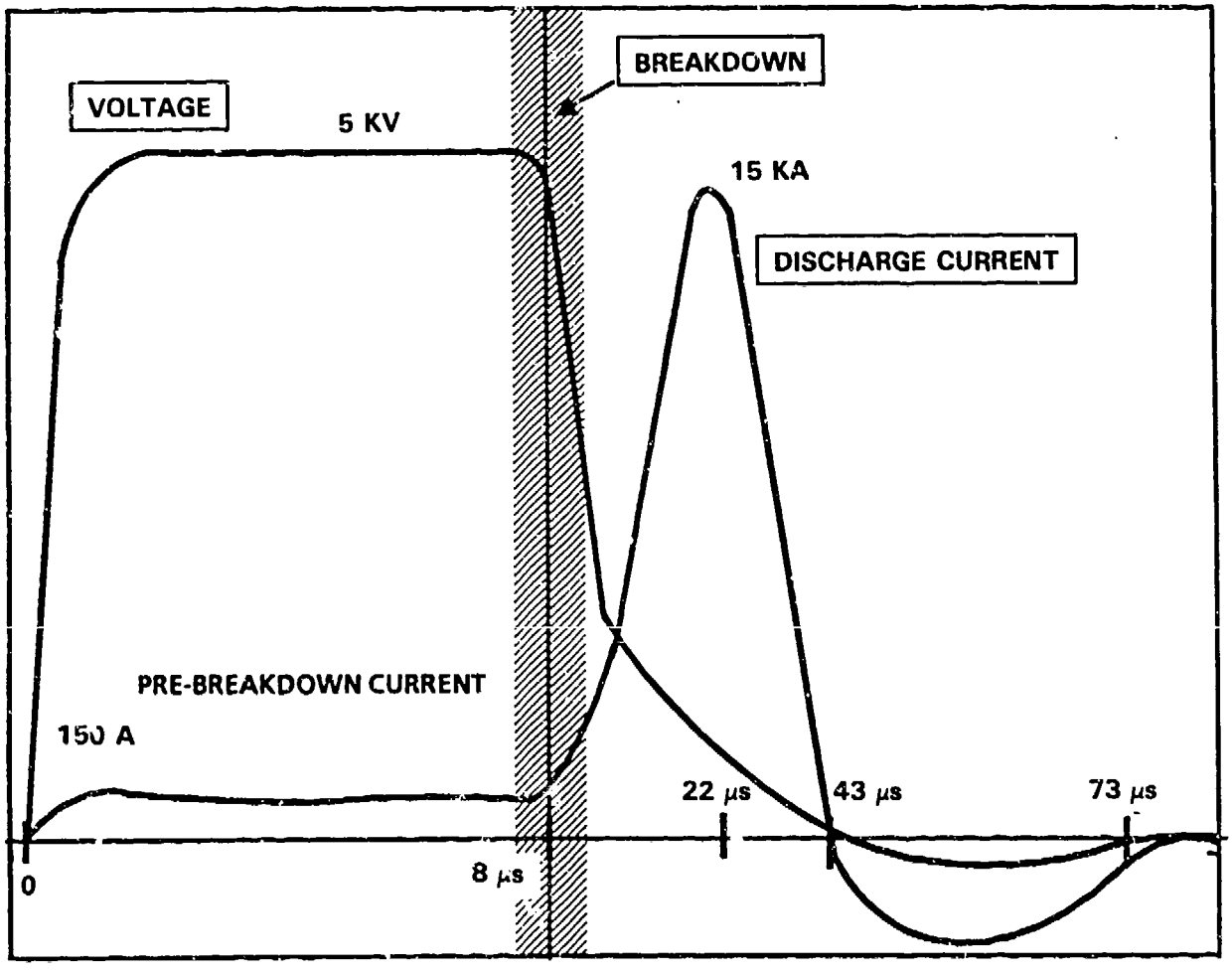

FIGURE 4-1. CURRENT AND VOLTAGE ILLUSTRATION FOR TYPICAL EXPERIMENT

TABLE 4-1. PRE-BREAKDOWN RESULTS

SAMPLE NUMBER	CAPACITOR μF	V_{CHARGE} kV	V_{SAMPLE} PRE-BREAKDOWN kV	I_{PEAK} PRE-BREAKDOWN A	ACTIVE ANODE DIAMETER mm	ENERGY TO BREAKDOWN J	TIME TO BREAKDOWN μs
3	54	5	4.8	216	12.7	4.63	7.16
4	54	5	4.75	164	12.7	4.4	8.12
5	54	5	4.7	98	11.5	3.2	16.44
6*	54	5	4.4	19	11.5	3.8	67.35
7*	54	5	4.5	95	11.5	4.75	16.0
8	0.4	5	4.3	174	11.5	N/A	-
9	0.4	9	5.25	1300	11.5	5.2	-
10†	0.4	9.9	5.18	1250	11.5	-	-
11	0.4	7	5.7	390	11.5	4.9	3.1
12	0.4	7	5.67	470	11.5	5.5	3.4
13	0.4	7	5.95	300	4.6	1.66	1.3
14	0.4	5.9	5.4	40	1.1	0.76	3.2

* The discharge circuit for samples 4 and 5 had series resistances of 49 Ω and 9.72 Ω respectively. These resistances served to limit the pre-breakdown current. The energy to breakdown was not significantly affected; however, the time to breakdown was increased considerably (67.4 and 16 μs respectively).

† The current profile for sample 10 was similar to that for sample 9. However the data for the current magnitude and hence the energy are not known because portions of the data were lost due to a malfunction with the oscilloscope.

Note: The shaded rows were used to compare the energy to breakdown with the active anode area.

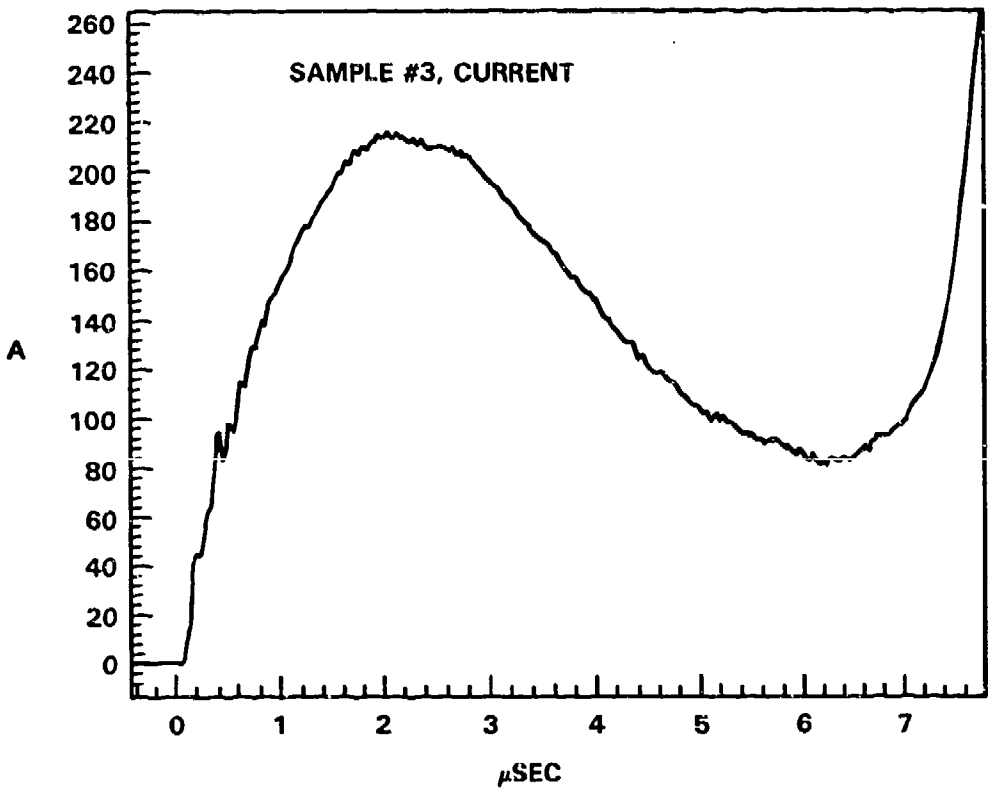

FIGURE 4-2. PRE-BREAKDOWN CURRENT

This behavior was observed for both capacitances charged to 5 kV. The sharp rise in the current at the end of the record marked the beginning of the discharge phase. The pre-breakdown current was observed to vary with changes in the series circuit resistance, the applied voltage and the active area.

SERIES CIRCUIT RESISTANCE

Samples 6 and 7 used 49 Ω and 9.72 Ω resistances respectively in series with the test sample. These resistances served to limit the pre-breakdown conduction (19 A and 95 A) and hence the time to breakdown (68 μs and 16.8 μs). The energy required for breakdown was not affected.

CAPACITANCE

No significant difference in the pre-breakdown current was observed when the capacitance was changed from 54 μF to 400 nF. The current observed for sample 8 (400 nF at 5 kV) is similar to that for sample 4 (54 μF at 5 kV). It was concluded that sample 8 did not breakdown because there was not enough energy transferred to the sample, i.e., less than 2.5 J.

VOLTAGE

Significant changes in the pre-breakdown current were observed when the voltage was increased. The conduction peak was more than doubled for samples tested at 7 kV.

Samples subjected to voltages of 9 kV and 9.9 kV (samples 9 and 10 respectively) did not display the typical current profile shown in Figure 4-2. The current and voltage records for sample 9 are shown in Figure 4-3. A large current (1.3 kA peak) was observed while the voltage was still high, i.e., during the pre-breakdown phase. A secondary rise in the current occurred after the voltage began to collapse. This anomalous current profile is the result of the combination of the smaller capacitance (400 nF) and the high charging voltage (9 kV). The high charging voltage induced a significant increase in the pre-breakdown current. Coincidentally, the sample began to breakdown at the pre-breakdown current peak; note that the voltage started to drop at this time. This subtle transition makes it difficult to accurately determine when dielectric breakdown occurred. The secondary rise in the current trace is the discharge current competing in parallel with the bulk conduction we normally associate with the pre-breakdown current. It is interesting to note that the energy to breakdown is ≈5.2 J, which is in accord with the other data. (See Table 4-1.)

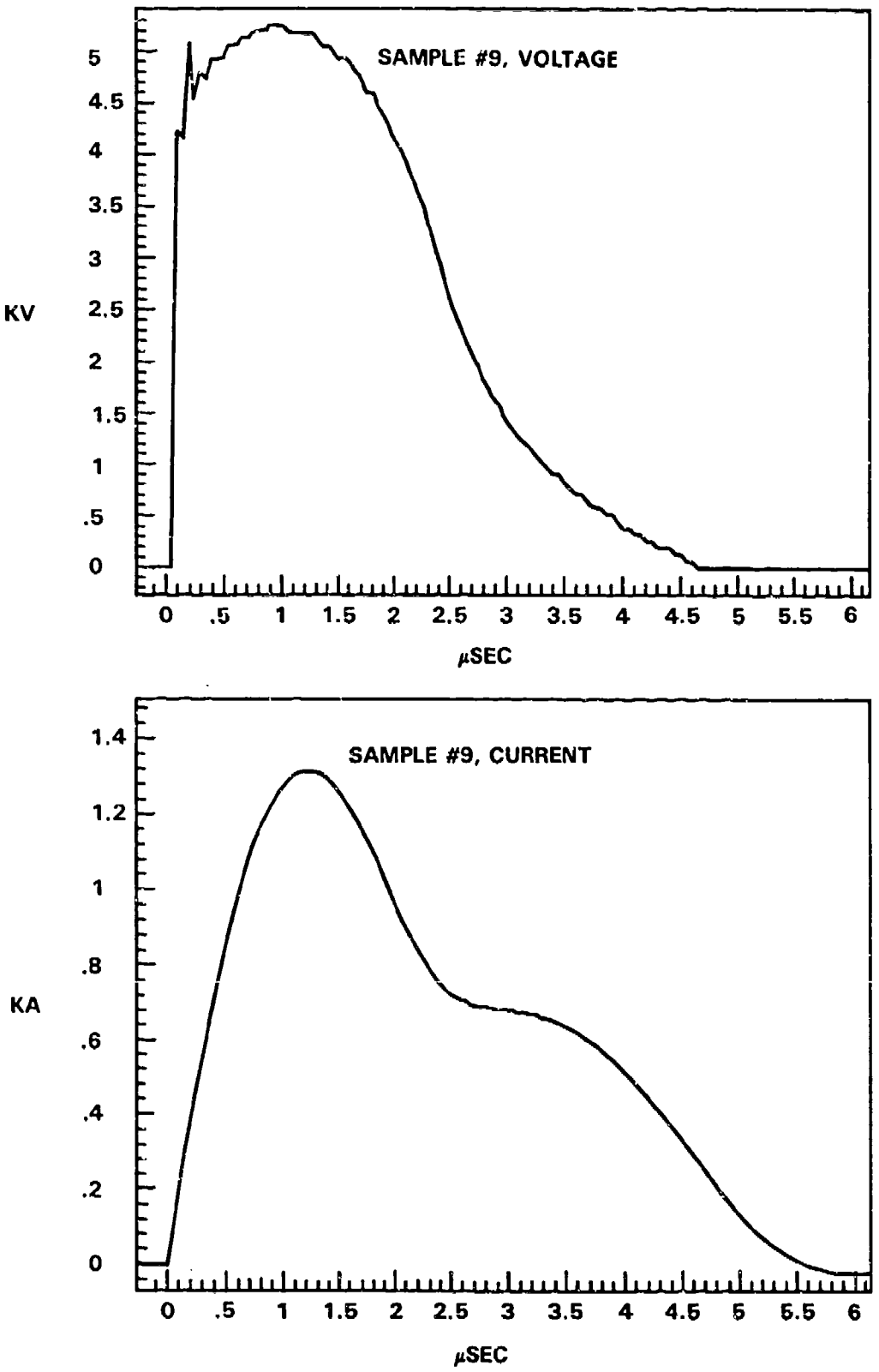

FIGURE 4-3. VOLTAGE AND CURRENT FOR SAMPLE 9, 400 nF AT 9 kV

VARIATION IN ACTIVE AREA

It was observed that the energy to breakdown did not vary significantly when the circuit was altered, i.e., the series resistance was added and the capacitance was changed. However, this energy did vary with changes in active area. The pre-breakdown current, the energy to breakdown and the time to breakdown were decreased by reducing the opening in the Kapton mask covering the anode.

A plot of "energy to breakdown" versus "active anode diameter" is given in Figure 4-4. The data used for this plot, from samples 11 through 14, represent experiments where the masking was well defined and the electrical circuit was comparable. Presenting the data in this fashion yields an increasing linear relationship between the energy required to cause breakdown and the active anode diameter. A least squares fit of the data indicated that the vertical intercept is 0.2. The standard error is 0.6; therefore, the vertical intercept is not significantly different from zero.

This relationship suggests that the pre-breakdown conduction is dependent on the electrode area in contact with the sample, hence the conduction is not singularly localized, i.e., one channel. Therefore, the pre-breakdown conduction may be the result of bulk conduction or multiple channels.

IGNITION PRIOR TO BREAKDOWN

A 0.4 μF capacitor was used to limit the energy delivered to the sample following dielectric breakdown. These experiments were used to determine if the energy deposited prior to breakdown was responsible for ignition. XPS studies showed no significant reaction in samples that did not breakdown or in regions extending beyond the arc channels of samples that did breakdown. Hence, reaction was confined to the arc channels formed after breakdown. The results concerning reaction in the arc channel are discussed in Chapter 5.

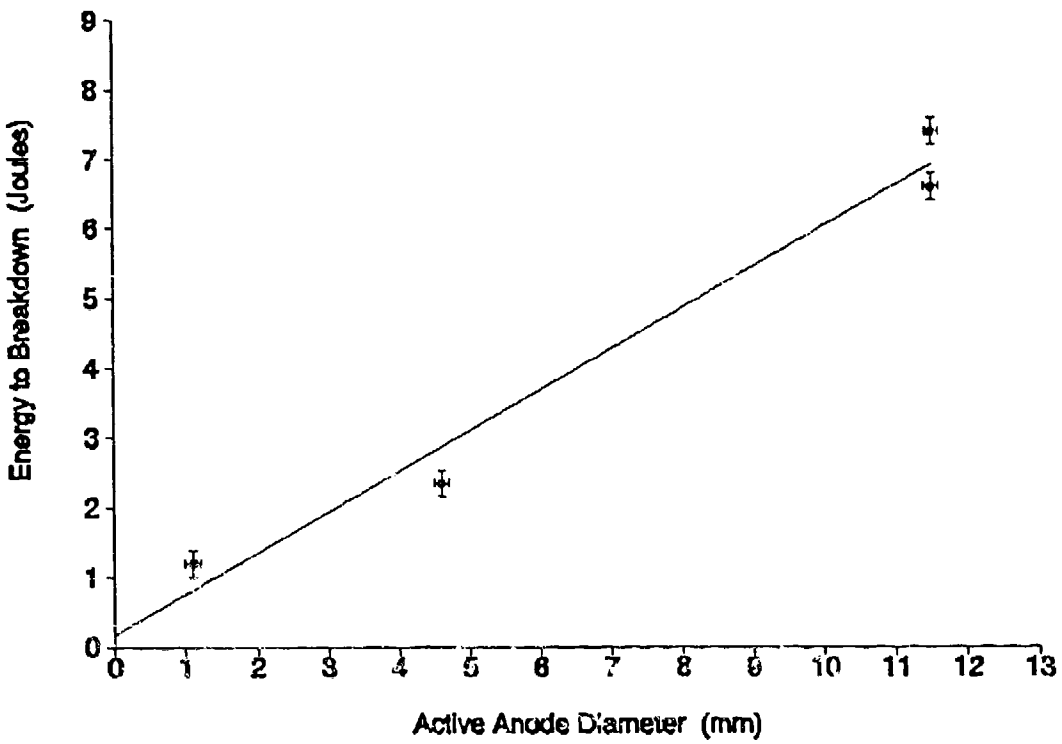

FIGURE 4-4. ACTIVE ANODE DIAMETER VS ENERGY TO BREAKDOWN

CHAPTER 5

IGNITION RESULTS

Table 5-1 displays data pertaining to the discharge phase following dielectric breakdown of each experiment. The energy and peak power data displayed in this table are those deposited in the arc channel following dielectric breakdown, i.e, after the voltage started to decline sharply. The results, though not perfect, are informative. The calculations of energy deposition during the arc discharge phase are in error due to the uncertainty of when dielectric breakdown occurred. These measurements could be improved by using a two-stage circuit, as described in one of our papers,[5] to separate the pre-breakdown and discharge phases.

EFFECT OF RESTRAINT

Figure 5-1 shows the physical results of an unrestrained sample on the left and that for a restrained sample on the right. PBXW-115 ignited and was completely consumed when 150 J was deposited in a restrained test cell which contained 6.35 mm thick explosive samples. The time to thermal explosion cannot be determined from these records, hence the energy required to initiate the sample was some fraction of 150 J. The restrained experiments used the retaining bolts shown in Figure 2-5, to keep the electrodes from being pushed away from the explosive surface. The test cell was pushed apart during the unrestrained experiments, thereby venting and presumably quenching the reaction. These unrestrained experiments allowed a study of the arc damage and the extent of reaction in the sample.

XPS RESULTS

XPS studies confirmed that thermal reaction was confined to the discharge path in unrestrained samples. No evidence of reaction was detected in areas beyond the arc channel for the recovered unrestrained charges.

XPS Spectra From Control Samples

Nitrogen (1s) photoelectron spectra from PBXW-115, HMX and AP are shown in Figure 5-2. The spectrum from PBXW-115 is seen

TABLE 5-1. POST BREAKDOWN RESULTS

SAMPLE NUMBER	CAPACITOR μF	V_{CHARGE} kV	DISCHARGE ENERGY J	PEAK POWER MW	RESTRAINT	REACTION	ARC DAMAGE
1	54	5	150	5.9	no	no	single channel
2	54	5	154	7.8	no	no	single channel
3	54	5	147	8.4	no	no	single channel
4	54	5	150	-	yes	yes	consumed
5	54	5	157	7	yes	yes	consumed
6*	54	5	-	-	yes	no	single channel
7*	54	5	-	-	yes	no	single channel
8	0.4		N/A	N/A	yes	no	N/A
9	0.4		7.4	1	yes	no	multiple channels
10†	0.4	9.9	-	2.4	yes	no	multiple channels
11	0.4	7	3.7	1.7	yes	no	multiple channels
12	0.4	7	3	1.3	yes	no	fluted channel
13	0.4	7	5.8	2.7	yes	no	single channel
14	0.4	5.7	5	1.9	yes	no	fluted channel

* The discharge circuit for Samples 4 and 5 had series resistances of 49 Ω and 9.72 Ω respectively. Current and voltage was not recorded after dielectric breakdown; therefore, the discharge energy is not available.

† The discharge energy for sample 10 is not known because portions of the current were lost due to a malfunction.

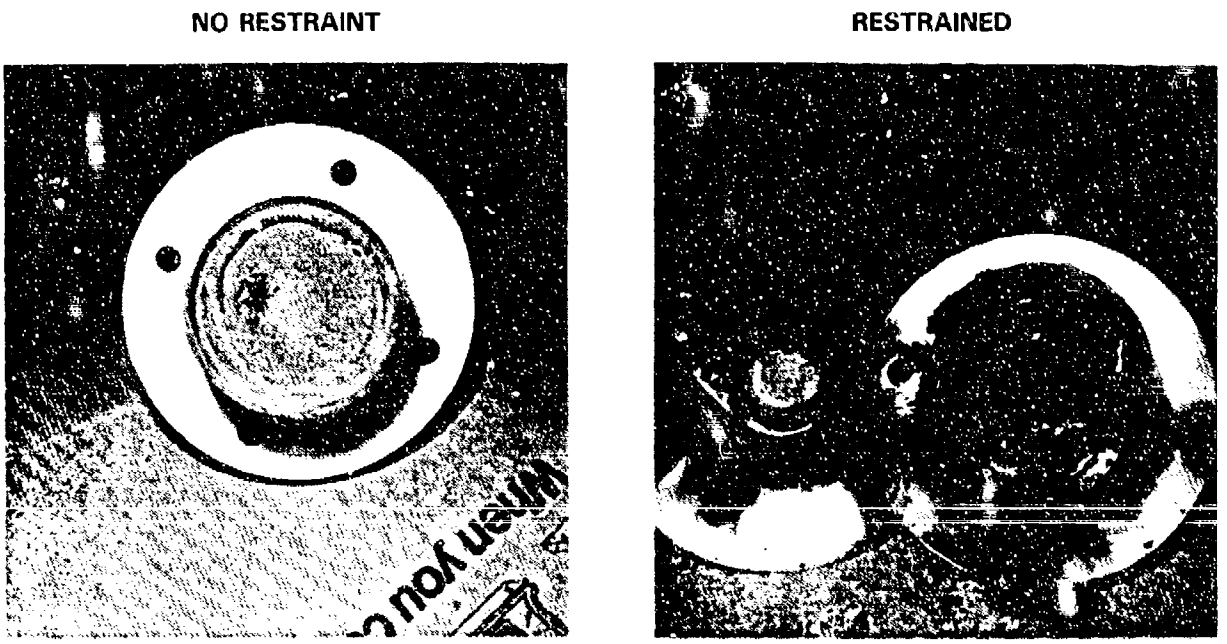

FIGURE 5-1. PHYSICAL RESULTS OF DISCHARGE EXPERIMENTS

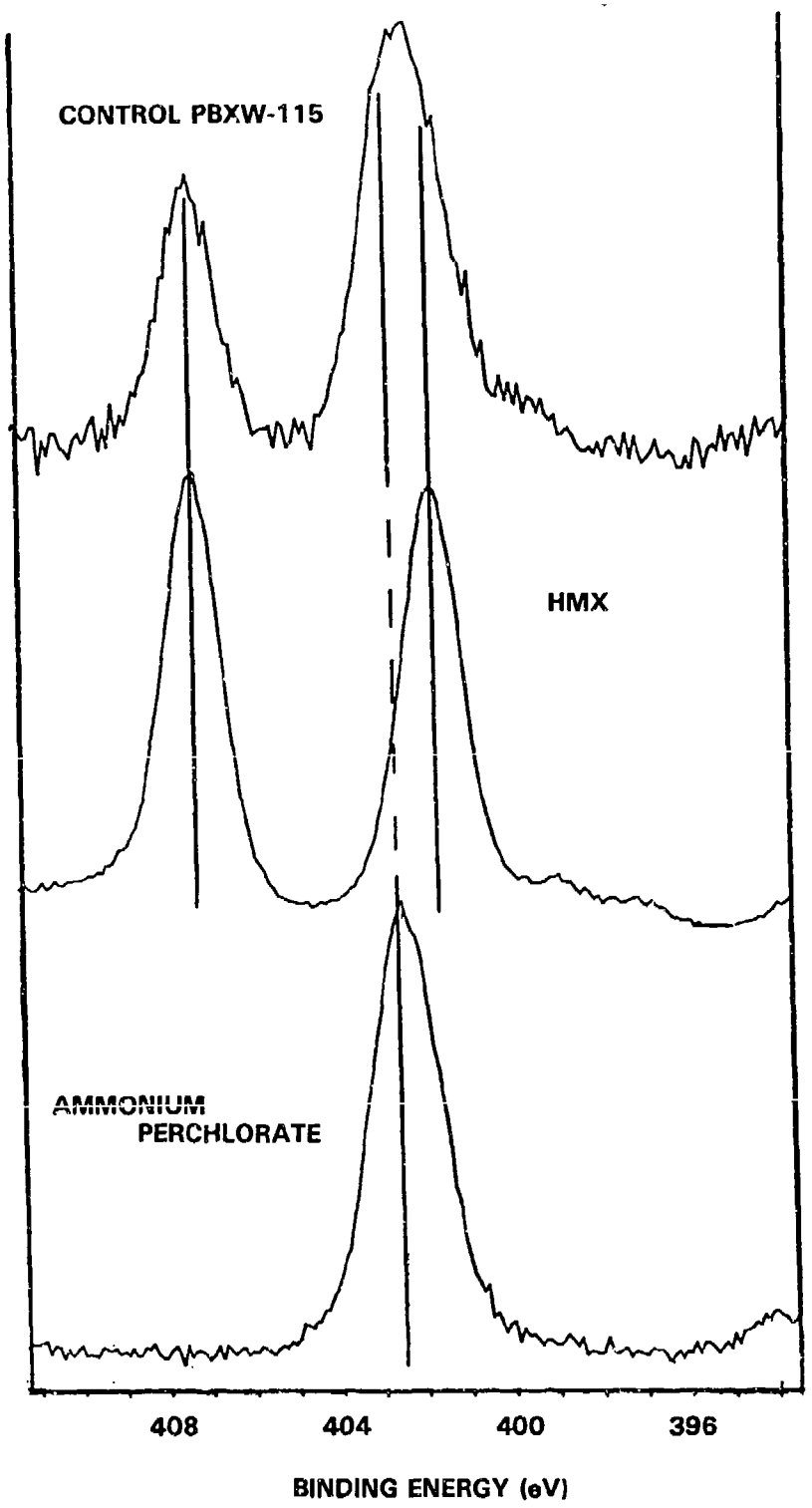

FIGURE 5-2. NITROGEN SPECTRA FOR AP, HMX AND PBXW-115

as the combination of those from HMX and AP. The two peaks from HMX originate from the nitramine group; the peak at 407.3 Ev is from the nitro nitrogen and the peak at 401.6 eV is from the amine nitrogen. The ammonium ion produces a peak at 402.5 eV, distinct from the HMX nitrogens.

The only chlorine containing component in the formulation is the AP. The binding energy of the highly oxidized perchlorate is 209.0 eV.

XPS Spectra From Discharged Samples

Chlorine and nitrogen spectra from recovered samples from test cells subjected to discharge energies of ≈150 and 5 J (samples 3 and 14 respectively) following breakdown are compared with control spectra in Figures 5-3 and 5-4. These spectra were taken from the region inside of the arc channel that was developed in each experiment.

Sample 3 (~150 J) demonstrates changes in chemistry in the discharge channel. The development of additional intensity in the N(1s) spectrum (Figure 5-3) at about 399.5 eV is suggestive of triazine chemistry arising from nitramine decomposition.[9] The decrease in the intensity of the portion of the N(1s) spectrum attributed to NH_4^+ suggests depletion in the relative amount of AP present within the sampling volume of the XPS.

Reaction in the discharge channel of sample 14 (5 J) is quite significant. Spectra of both the N(1s) and Cl(2p) had very low signal intensity, suggesting a significant surface depletion of these elements compared to a fresh cut surface from a control sample. Of the N and Cl that did remain near the surface and visible to the XPS, chemical changes were also observed. Intensity from the NH_4^+ in the N(1s) spectrum is virtually gone. Chlorine (2p) was also very weak.

The extent of reaction in sample 14 appeared to be greater than that observed in sample 3, despite the ten fold higher energy deposition into sample 3. Total energy density within a discharge arc channel is the most important factor. Owing to the possibility of unseen channels, and possible variation in the channel size, there is a possibility that the energy density in the channel investigated from sample 14 was greater than that from sample 3.

An alternative evaluation of these results would suggest that the extent of reaction was so great in the 150 J case that all trace of material was lost do to complete reaction exposing the slightly reacted bulk.

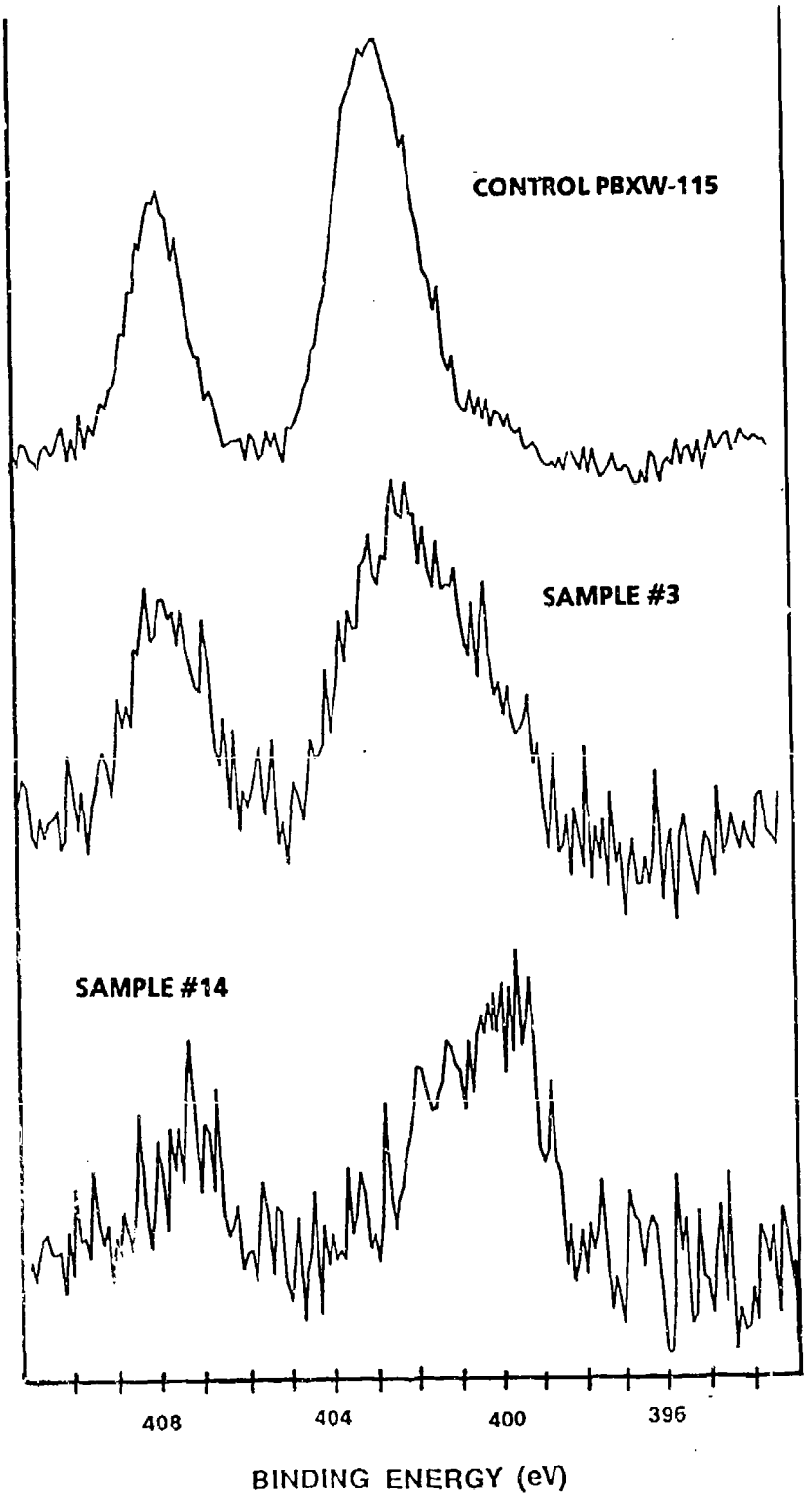

FIGURE 5-3. NITROGEN SPECTRA FOR SAMPLES 3 AND 14

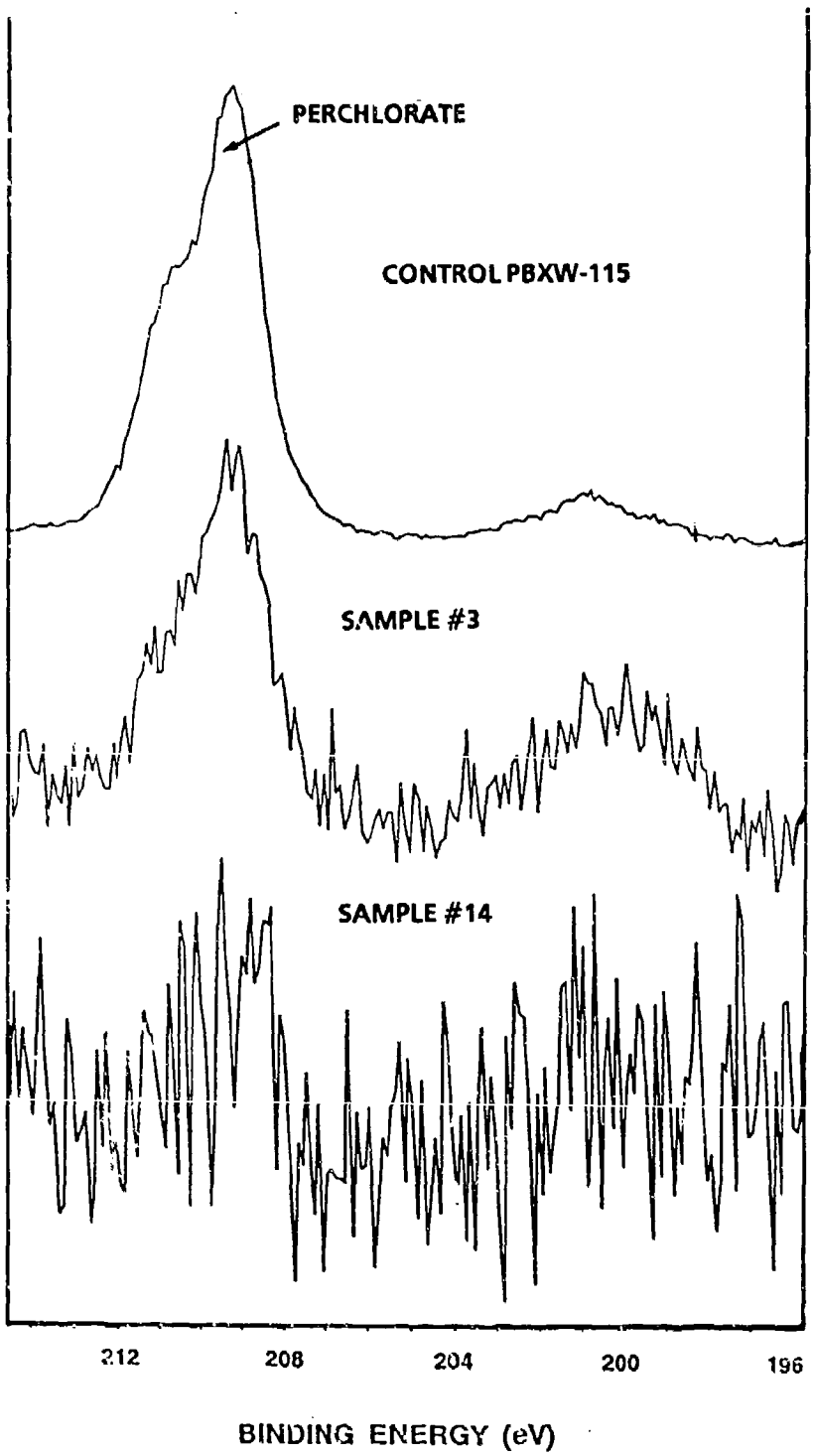

FIGURE 5-4. CHLORINE SPECTRA FOR SAMPLES 3 AND 14

Summary

These results indicate that reaction occurred in the arc channel for both samples, i.e., for an energy deposition of 150 and 5 J. Similar tests performed on the material outside of the arc channel did not display any signs of reaction. This observation suggests that the energy density in the arc channel is sufficient to cause reaction independent of the deposition energy.

PHYSICAL NATURE OF DISCHARGE CHANNELS

Photomicroscopy shows that the arc channel diameter was ≈1 mm in recovered samples (from test cells subjected to 150 J deposition). Multiple channels and convoluted discharge shapes, discussed below, were observed in other samples subjected to lesser energy depositions. These results show that a complete analysis of localized energy in discharge channels would be complicated. However, for the discussion describing shock ignition in Chapter 6, a single cylindrical discharge channel is considered.

Figure 5-5 demonstrates two well separated paths in a sample subjected to ≈3.7 J (sample 11) following breakdown. The sequencing of these paths cannot be determined, however, it is reasonable to assume that current passed through both at an early stage in the discharge. Later, the path on the right became the major current carrier, demonstrating the greatest amount of damage. The shape of the major discharge path is suggestive of a trident by the multiple branches leading to the one surface. Figure 5-6 illustrates a highly unusual discharge path observed during this study. What appears to have been a sheet of discharge went through the sample directly along the circumference of the electrodes. The length of this discharge is ≈8.5 mm. Evidence of more intense discharge channels is observed within the generally charred region.

ENERGY AND POWER

The question is: What is more important for ignition, the energy or the power? Note that samples 4 through 13 (representing energy depositions from 3 to 157 J) were restrained, yet no ignition occurred unless ≈150 J was deposited. However, the energy may not be the critical parameter. The peak power during the discharge phase for the high energy experiments (samples 1 through 5, 54 μF) was $\geq$ 6 MW, and that for the low energy experiments (samples 9 through 13, 400 nF) was $\leq$ 2.5 MW. Sample 8 was excluded from this comparison because it did not breakdown.

FIGURE 5-5. CROSS SECTION OF ARC CHANNELS FROM SAMPLE 11

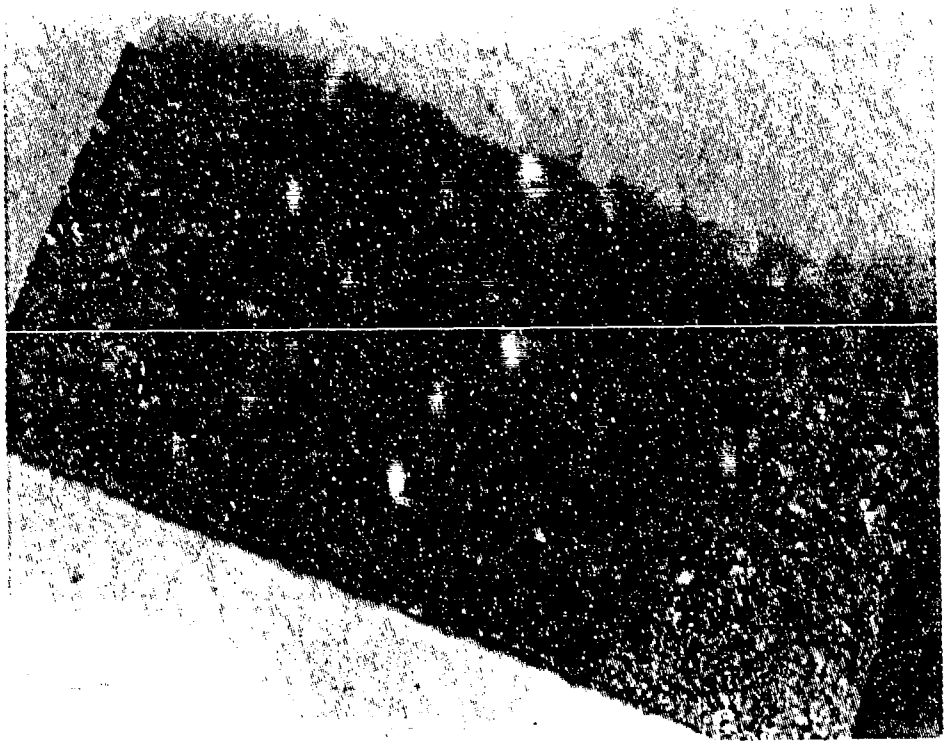

FIGURE 5-6. CROSS SECTION OF ARC CHANNELS FROM SAMPLE 9

Samples 9 and 10 represent another interesting aspect of the problem. The high charging voltages (9 and 9.9 kV respectively) for these experiments enhanced the pre-breakdown conduction, hence, they displayed powers comparable to the high energy experiments (6.8 and 7.8 MW respectively) during the pre-breakdown phase. The transition in the current profile at breakdown was impossible to detect since the resistance associated with each phase was comparable. These two samples did not ignite because the electric energy density was relatively low. During the pre-breakdown phase, the energy density is low because the conduction is over the active volume established by the electrode masking. During the discharge phase the energy was dissipated in an array of multiple arc channels, like that displayed in Figure 5-6. These multiple channels served to dissipate the energy over a wider volume, perhaps mitigating against ignition. The effect of the power and the arc dynamics on ignition sensitivity is discussed in Chapter 6.

CHAPTER 6

SHOCK IGNITION THEORY

Walker and Wasley's energy fluence or $P^2\tau$ criterion has proved to be a useful tool for predicting explosive sensitivity to the shock initiation of detonation.[10,11,12,13] The energy fluence, E, is approximated by:

$$E = \frac{P^2 \tau}{U_s \rho_0} \qquad (6\text{-}1)$$

where P is the peak shock stress at the initial impact surface in the unreacted explosive, τ is the shock pulse width at one-half peak stress, U_s is the shock velocity and ρ_0 is the initial density. The criterion for detonation is met when an applied stress is sufficient to exceed a critical energy fluence.

REACTION THRESHOLD DEFINITIONS

Liddiard and Forbes[14] have extended the $P^2\tau$ criterion to define and compare thresholds for two states of shock induced reaction. The first is called *first reaction*, originally called the burning threshold, where the first evidence of reaction is observed. The second is *sustained ignition*, where deflagration could grow to detonation in a sufficiently large explosive sample. This state of reaction corresponds to deflagration velocities greater than ≈1 km/s. *First reaction* is typically of less vigor and occurs at a lower initiating energy fluence than *sustained ignition*, and it will not grow to detonation. The two thresholds were found to be significantly different for cast explosives but relatively close for pressed explosives.[15]

APPLICATIONS TO ESD

Energy fluences, determined for quasi-planar shocks, are assumed to be comparable to those of cylindrical shocks generated by explosive ignition due to electrical discharges. In this way an analysis of the shock loading from an electrical discharge, using the energy fluence criterion, can determine the likelihood of *first reaction* in cylindrical arc channels.

It is hypothesized that the deposition of electrical energy causes a thermal explosion of the material in a single discharge

channel. The diameter of the channel depends on the electrical energy deposited.[16] The channel explosion will only initiate the surrounding explosive if its diameter is larger than some critical value, i.e., if it generates a pulse of sufficient duration. An order of magnitude calculation for the critical diameter will be presented below.

THEORY

Shocks are typical for any arc discharge and in certain cases, e.g., current rates of 10^{11} A/s, the pressures can exceed those produced by explosives.[17] However, within the deposition energies of interest for ESD it is expected that the chemical energy density in the arc channel greatly exceeds the electrical energy density. Hence, it is proposed that the electric arc, by itself, does not produce a significant pressure pulse. However, the arc does induce thermal decomposition that leads to thermal explosion of the material within the arc channel. This is supported by the X-ray Photoelectron Spectroscopy (XPS) data which do not indicate any reaction beyond the discharge channel.[18] The thermal explosion launches a cylindrical shock wave into the surrounding unreacted explosive. Thus the electric arc triggers the thermal decomposition, but it does not contribute to the subsequent shock initiation process.

The following analysis is a refinement of previous calculations[18] of the shock pulse width required to ignite explosives via a cylindrical thermal explosion.

Shock Pressure

By definition a thermal explosion in the discharge channel occurs at constant volume. From a polytropic equation of state[19] for the gas products, the explosion pressure, P_e, is exactly half the Chapman-Jouguet pressure, P_j. Therefore, P_e is 6.15 GPa for this case since P_j = 12.3 GPa for PBXW-115.[20]

The shock pressure, P_s, delivered to the unreacted explosive is determined from the intersection of the reacted thermal explosion isentrope[19] and the unreacted shock Hugoniot[20] which are given below respectively.

$$u_p = -\frac{2}{1-\gamma}\sqrt{\frac{\gamma P_e}{\rho_0}}\left[\left(\frac{P}{P_e}\right)^{\frac{\gamma-1}{2\gamma}} - 1\right] \quad (m/s) \tag{6-2}$$

$$P = \rho_0 u_p (1.77\, u_p + 2377) \quad (Pa) \tag{6-3}$$

The coefficient $\gamma = 3.34$ is a constant of the polytropic equation of state and $\rho_o = 1790$ kg/m^3 is the initial density for PBXW-115.[19] The particle velocity, u_p, in the channel is initially zero since thermal explosion is a constant volume reaction. It is assumed that the energy deposited from ESD after thermal ignition is small in comparison to the heat of reaction. Therefore, the reactive isentrope in P-u_p space intersects the coordinates (P_c, 0) and intersects the Hugoniot at $P_s = 3.35$ GPa.

Shock Velocity

The shock velocity, U_s, in the unreacted explosive is found to be 3.36 km/s from the U_s-u_p relation at $P_s = 3.35$ GPa.

$$U_s = 1.77\,u_p + 2377 \quad (m/s) \tag{6-4}$$

Shock Pulse Width

The shock pulse width at half peak pressure, τ, is approximately equal to the time it takes the first rarefaction to travel to the center of the discharge channel and back again to meet the expanding channel wall. The deposited electrical energy governs τ by determining the initial arc channel diameter. Consequently, an increase in channel size increases the energy fluence and the possibility of ignition beyond the channel.

In this study, only simple flow effects are used to estimate the transit times of the waves in the arc channel, i.e., the attenuation of the shock pulse is ignored. The time-distance plot in Figure 6-1 illustrates the motion of the rarefaction front, channel expansion and shock front. Each front is labeled by its corresponding velocity. The shock front expands into the surrounding unreacted explosive from the channel wall at a velocity U_s, the channel wall expands at the particle velocity u_p and the initial rarefaction front travels towards the center of the channel at a velocity c. The time the initial rarefaction takes to cross to the center of the channel is:

$$t_1 \sim \frac{r}{c} \tag{6-5}$$

where r is the radius of the channel and c is the initial sound speed in the channel. The rarefaction velocity is given by $(c + u_p)$, however, the velocity of the initial rarefaction is equivalent to c because u_p is initially zero. Now c can be obtained from the derivative of the isentrope for the explosive's product gases,

$$c^2 = \left[\frac{dP}{d\rho}\right]_s \tag{6-6}$$

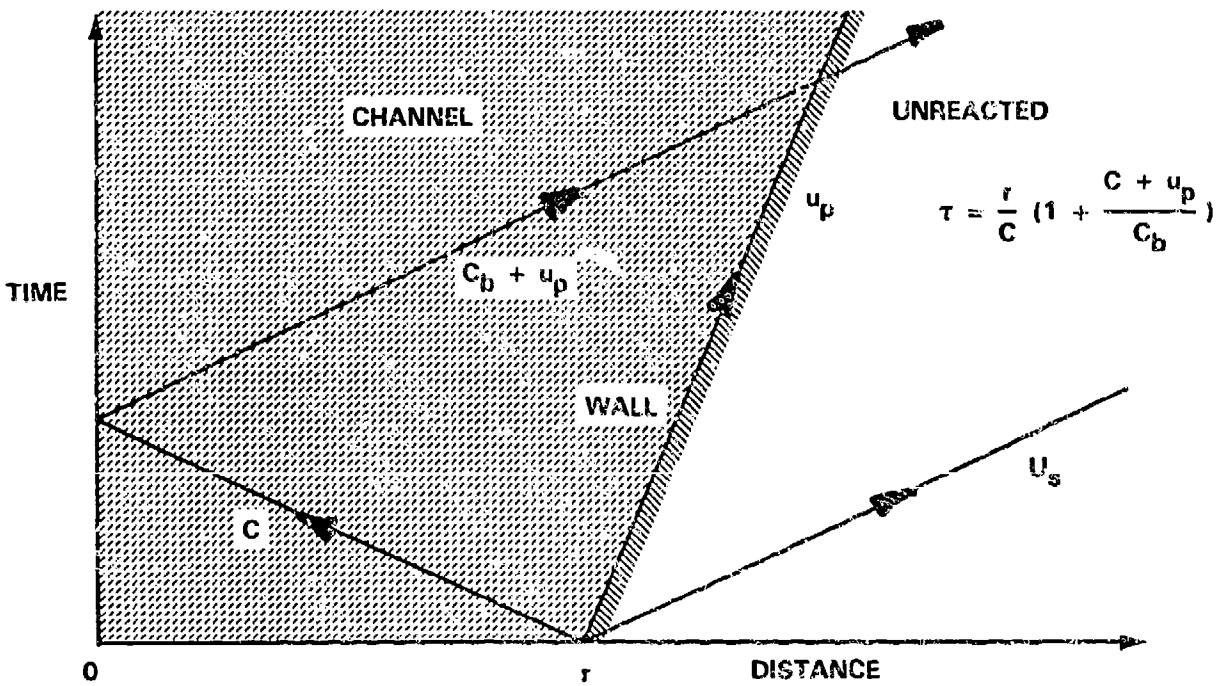

FIGURE 6-1. SIMPLE HYDRODYNAMICS OF A THERMALLY EXPLODED ARC CHANNEL

where the isentrope is defined as

$$P = P_e\left(\frac{\rho}{\rho_0}\right)^{\gamma} \tag{6-7}$$

Evaluating the derivative at ρ_o yields

$$c = \sqrt{\frac{P_e\gamma}{\rho_0}} \tag{6-8}$$

Therefore, c ≈ 3.4 km/s and the arc channel diameter for reaction was found to be ≈1 mm, so t_1 ≈ 150 ns.

The rarefaction is reflected at the center of the channel as a result of the shock impedance mismatch. The cylindrical imploding wave leaves a pressure $P_b = P_s = 3.35$ GPa behind the front as it propagates towards the center of the channel. The impedance mismatch occurs where the rarefaction arrives at a boundary between the two pressure states, P_e and P_b, at the center of the channel. The reflected rarefaction propagates back through the pressure state P_b at a different velocity $(c_b + u_p)$ where $u_p \approx 0.56$ km/s. The velocity u_p was obtained at the intersection of the explosive isentrope, and the unreacted Hugoniot at $P_s = 3.35$ GPa. The new sound speed, c_b, is evaluated as before.

$$c_b = \sqrt{\frac{P_b\gamma}{\rho_b}} \tag{6-9}$$

The density $\rho_b = 1495$ Kg/m^3 is determined from the above isentrope, therefore, $c_b = 2.7$ km/s and the rarefaction velocity $(c_b + u_p) \approx 3.3$ km/s.

It is assumed that after thermal ignition any significant expansion of the channel comes from mechanical flow and not arc erosion. Therefore, the wall has expanded at a rate of $u_p \approx 0.56$ km/s after the initial thermal explosion, and the wall has then moved out $(u_p\ r/c)$ at the time of reflection. The rarefaction takes a time t_2 to meet the wall after reflection at the center of the channel.

$$t_2 = \frac{r + \frac{u_p r}{c}}{c_b} \tag{6-10}$$

Consequently, the approximate shock pulse width is

$$\tau = \frac{r}{c}\left(1 + \frac{c + u_p}{c_b}\right) \qquad (6\text{-}11)$$

The arc channel diameter for reaction was found to be ≈1 mm and the equivalent pulse length τ was calculated to be ≈360 ns.

Energy Fluence

The energy fluence for ESD ignition in PBXW-115 is thus estimated to be 6.7×10^5 J/m^2 using $P^2\tau$. Note that the attenuation of shock waves was not taken into account in this calculation. Hence, the calculated fluence is the maximum the sample would receive.

This fluence can be compared with fluence data from the Modified Gap Test (MGT)[20] for PBXW-115. The MGT energy fluence for *first reaction* is 5×10^5 J/m^2 and the fluence required for *sustained ignition* is 6×10^6 J/m^2. This implies that the ESD discharge would lead to deflagration but not detonation. To obtain detonation the discharge channel τ would have to be increased tenfold. The diameter is a function of deposited energy but the energy required to generate a 10 mm channel in PBXW-115 has not yet been determined.

EFFECT OF POWER AND ARC DYNAMICS

It is proposed that ESD ignition sensitivity is dependent on the hydrodynamics of the arc channel growth and the thermodynamics leading up to the thermal explosion. The above analysis indicates that the degree of reaction deperds on the arc channel diameter at the time of thermal explosion. We submit that a single arc channel offers sufficient localization of the electrical energy to cause reaction within the channel, i.e., the thermal explosion. It is feasible that the thermal explosion could occur before the arc channel attains the critical diameter required for continued reaction, i.e., *sustained ignition*. If this occurs then subsequent deposition of electrical energy in this arc channel may not result in a *sustained reaction*. That is to say that the electrical energy is now being deposited down an open hole.

The thermal explosion likely has an incubation time once a sufficient energy density is achieved. This incubation period could provide the time needed to achieve the critical arc channel diameter if the rate of energy deposition, i.e., the electrical power, is high enough. So the electrical power is crucial in ESD ignition sensitivity.

It should be noted that if the energy is dispersed among several arc channels, the individual channels may not reach the critical diameter for ignition.

Chapter 7

DISCUSSION

Before the ESD problem can be resolved, the following four items need to be addressed: (1) the electric energy transfer associated with insulated cases, (2) the effect of the discharge profile on the reaction sensitivity, (3) the effect of confinement on the sensitivity and (4) an ignition mechanism for explosives. This report offers data for the latter three.

TEST METHODS

Conventional tests are poorly designed in terms of electrical efficiency and power transfer. These tests take for granted that the deposition energy is equivalent to the energy stored on the capacitor. In reality, a small fraction of the stored energy is deposited in the sample due to losses in the circuit. To make accurate measurements of ignition energy good electrical diagnostics should be used, such as the techniques reported here.

Chapter 2 includes a discussion of diagnostic tools which can be used to obtain accurate power and energy depositions.

POWER PROFILE

Circuit design is important. The capacitance, the parasitic inductance and the resistance associated with any circuit determines the rate at which the energy is transferred. Conventional test equipment include large parasitic circuit inductances whereas warhead cases do not. These inductances dominate the rate of transfer of the electrical energy to the explosive, so the test apparatus does not simulate real hazard conditions. Moreover, the effect on ESD ignition sensitivity due to varying the energy deposition rate, i.e., the power profile, has not been determined.

The hypothesis that can be drawn from the analysis in Chapter 6 is that the power associated with the electrical discharge is important to the ESD ignition sensitivity.

CONFINEMENT

Recent studies by Hodges[21] suggest that an increase in confinement can decrease the critical ESD ignition energy by several orders of magnitude. Hodges reported that the threshold ignition energy for a PBAN composite aluminized propellant was reduced from 3 J to 70 mJ when subjected to a static nitrogen pressure of 4.67 MPa (700 psig).

Our own results suggest the same trend with confinement. *Sustained ignition* occurred in PBXW-115 only when the samples were restrained. This restraint allowed a small pressure rise to occur after ignition by ESD. The restraint was provided by holding the electrodes against the explosive via retaining bolts. The work performed thus far has used a sample size 1.75 inches in diameter and 0.25 inch thick, i.e., well below the critical diameter for PBXW-115. The fear is that the sample could be ignited by smaller energies if it is larger or sufficiently confined.

Results from the Royal Armament Research Development Establishment (RARDE), Waltham Abbey, UK,[22] show ignition energies, to an unknown degree of reaction, in 10's of mJ for propellants that have similar compositions to PBX explosives. These results are disturbing when compared to our own results. The only successful *sustained ignition* experiments for PBXW-115, thus far, have been when a total energy of 150 J was deposited. The precise time of ignition, and hence the ignition energy, was not determined in these experiments. We believe that the magnitude of the electric power (≈8.4 MW peak) was the crucial element of these experiments, and the actual energy to ignition was several orders of magnitude lower than 150 J. The discrepancies between the British data and our own are likely due to differences in confinement as well as rate of energy deposition.

PRESENT THEORY

Shock energy fluence data for PBXW-115 were used to show that mechanical shock is the probable cause of ignition due to an electrical discharge. It was hypothesized that the thermal explosion of the material in the electrical discharge channel transmits a shock wave into the unreacted explosive. The explosive is subsequently shock initiated into reaction. A minimum energy fluence, E, is required to cause *first reaction** in the surrounding explosive.[15]

---

* *First reaction* is the first observable sign of reaction in the shock initiation experiments reported in Reference 15.

$$E = \frac{P_s^2 \tau}{\rho_0 U_s} \qquad (7\text{-}1)$$

where P_s is the shock pressure, τ is the shock pulse width, ρ_0 is the initial density and U_s is the shock velocity.

P_s and U_s are defined by thermal explosion theory and shock impedance mismatching. It is assumed that the electrical energy required to initiate the thermal explosion is small compared to the heat of reaction, and that the electrical energy deposited after thermal explosion has little effect on the shock. Therefore, the degree of reaction caused by ESD ignition is dependent on τ which is equal to the time it takes the first rarefaction to travel to the center of the discharge channel and back again to meet the expanding channel wall. Hence, τ is a function of the arc channel radius. The channel diameters formed by electrical discharge were found to be consistent with shock wave energy fluences necessary for *first reaction*.

FUTURE WORK

Further work is required to determine the minimum electrical discharge energy in the arc channel necessary to initiate thermal explosion. This could be accomplished by measuring pressure as a function of time during an ESD experiment. These measurements would determine when thermal ignition in the channel and shock ignition in the surrounding material occur with respect to the electrical discharge. These experiments would also yield experimental corroboration of the pressure pulse magnitude and duration with that from the simple theory presented here.

CHAPTER 8

CONCLUSIONS

PBXW-115 was found to conduct at electric field strengths exceeding ≈500 kV/m. An energy density of ≈8 x 10^6 J/m^3 was required to induce catastrophic breakdown. Low energy experiments, 3 to 13 J, showed that the energy deposited prior to breakdown was not responsible for ignition.

XPS studies confirmed that thermal reaction was confined to the discharge channel. The highly localized energy deposition in an arc channel likely raises the local temperature above that required for thermal ignition. However, a sustained reaction was not observed unless the sample was restrained. This suggests that mechanical shock may be responsible for ESD ignition.

A simple analytical model has demonstrated that if ESD induces a thermal explosion in an arc channel, then the reaction can be carried to the surrounding mass of unreacted explosive. The analysis given in this report has shown that the thermal explosion of a 1 mm diameter cylinder of PBXW-115 appears to be sufficient to induce *first reaction*, i.e., a rapid deflagration that is too weak to accelerate to detonation.

The electrical discharge energy serves to define the diameter of a discharge channel and, therefore, the shock pulse width. Further work is required to determine the minimum electrical discharge energy in the arc channel necessary to initiate thermal explosion. This could be accomplished by measuring pressure as a function of time during an ESD experiment. These measurements would determine when thermal ignition in the channel and shock ignition in the surrounding material occur with respect to the electric discharge. These experiments would also yield experimental corroboration of the pressure pulse magnitude and duration with that from the simple theory presented here.

REFERENCES

1. Technical Investigation of 11 January 1985 Pershing II Motor Fire, U.S. Army Missile Command, Redstone Arsenal, AL, Technical Report RK-85-9, Jun 1985.

2. "M592 Mishap Report, 29 December, 1987," TRW-25762, Thiokol Inc., Strategic Operations, Oct 1989.

3. Hodges, R.V. and Zeitke, B.R., "Electrostatic Charge Density Production on a Rocket Motor by Normal Handling Operations," in Proceedings of the 1990 JANNAF Propulsion Systems Hazards Subcommittee Meeting, Laurel MD, Mar 1990.

4. Lee, R.J., Static Dielectric Breakdown Strength of Condensed Heterogeneous High Explosives, NSWC TR 85-380, Jun 1987.

5. Lee, R.J. and Tasker, D.G., "The Acquisition of Definitive ESD Sensitivity Data and a New Test Method," in Proceedings of the 1987 JANNAF Propulsion Systems Hazards Subcommittee Meeting, Huntsville AL, Mar 1987.

6. Schwab, A.J., High-Voltage Measurements Techniques, MIT Press, Cambridge, MA, and London, England, 1972.

7. Tasker, D.G., The Properties of Condensed Explosives for Electromagnetic Energy Coupling, NSWC TR 85-360, Oct 1985.

8. Sharma, J., "X-Ray Photoelectron Spectroscopic (XPS) Detection and Identification of Explosives Residues," in Proceedings of the International Symposium on the Analysis and Detection of Explosives, FBI Academy, Mar 1983, p. 181.

9. Beard, B.C., "X-Ray Radiation Decomposition of (RDX), Cyclo-1,3,5-trimethylene-2,4,6-trinitramine, at Low Temperature: Initial Reaction Steps," Propellants Explosives and Pyrotechnics, Jan 1990.

10. Walker, F.E. and Wasley, R.J., "Critical Energy for Shock Initiation of Heterogeneous Explosives," Explosivstoffe, No. 1, 1969, pp. 9-13.

11. Walker, F.E. and Wasley, R.J., "Initiation of Nitromethane with Relatively Long-Duration, Low Amplitude Shock Waves," Combustion and Flame, No. 15, 1970, pp. 233-246.

12. Walker, F.E. and Wasley, R.J., "Initiation Patterns Produced in Explosives by Low-Pressure, Long-Duration Shock Waves," Combustion and Flame, No. 22, 1974, pp. 53-58.

13. Walker, F.E. and Wasley, R.J., "A General Model for the Shock Initiation of Explosives," Propellants and Explosives, No. 1, 1976, pp.73-80.

14. Liddiard, T.P. and Forbes, J.W., A Summary Report of the Modified Gap Test and the Underwater Sensitivity Test, NSWC TR 86-350, Mar 1987.

15. Liddiard, T.P., Forbes, J.W. and Price, D., "Physical Evidence of Different Chemical Reactions in Explosives as a Function of Stress," in Proceedings of Ninth Symposium (International) on Detonation, Portland, OR, 1989, pp. 1235-1242.

16. Mel'nikov, M.A. and Nikitin, V.V., "Determination of the Kinetic Parameters of RDX Initiated by an Electrical Spark," Fizika Goreniya i Vzryva, Vol. 8, No. 4, 1972, pp. 591-593.

17. Yu. V. Skvortsov, V. S. Komel'kov and N. M. Kuznetsov, "Expansion of a spark in a Liguid," Soviet Physics Technical Physics, Vo. 5, pp. 1100, 1960.

18. Lee, R.J., Tasker, D.G., Forbes, J.W., Beard, B.C. and Sharma, J., "Shock Ignition of an Explosive Due to Electrostatic Discharge (ESD)," in Proceedings of APS Conference on Shock Waves in Condensed Matter, Albuquerque, NM, Aug 1989.

19. Duvall, G.E. and Fowles, G.R., "Shock Waves," High Pressure Physics and Chemistry, Vol. 2, ed. R. S. Bradley (Academic Press, New York, 1953), pp. 209-291.

20. Liddiard, T.P. and Forbes, J.W., NSWC, White Oak, "MGT Test Data and Other Information on PBXW-115," private communications, Jul 1989.

21. Hodges, R.V. and McCoy, L.E., "Threshold Ignition Energy for an Internal Electrical Discharge in Propellant," in Proceedings of the 1990 JANNAF Propulsion Systems Hazards Subcommittee Meeting, Laurel, MD, Mar 1990.

22. Brian Hammant, RARDE Waltham Abbey, United Kingdom, ESD ignition experiments conducted at RARDE, private communications, Jul 1988.

DISTRIBUTION

	Copies
Chief of Naval Research	
Attn: ONR 1132P (R. Miller)	1
ONT 20T (L. V. Schmidt)	1
ONT 213 (D. Siegel)	1
ONT 23 (A. J. Faulstich)	1
ONT 232 (D. Houser)	1
800 N. Quincy Street, BCT 1	
Arlington, VA 22217-5000	
OUSDRE/R&AT-MST	
Attn: R. Siewart	1
The Pentagon	
Washington, DC 20301	
OUSDRE/TWP-NW&M	
Attn: D. Anderson	1
The Pentagon	
Washington, DC 20301	
OUSDRE/TWP--OM	
Attn: G. Kopcsak	1
The Pentagon	
Washington, DC 20301	
USD(A)/DDRE (R/AT/ET)	
Staff Specialist for Weapons Technology	
Attn: F. Menz	1
The Pentagon	
Washington, DC 20301	
OASN/RE&S	
Attn: Surface Warfare	1
Air Warfare	1
Subs/ASW	1
Navy Department	
Washington, DC 20301	

	Copies
Chairman	
Department of Defense Explosives Safety Board	
Attn: 6-A-145	1
DDESB-KT	1
Hoffman Building 1	
2461 Eisenhower Avenue	
Alexandria, VA 22331	
Chief of Naval Operations	
Attn: OP-098	1
OP-981	1
OP-982	1
OP-983	1
OP-987	1
OP-02T	1
OP-22	1
OP-225	1
OP-32	1
OP-35	1
OP-37	1
OP-374	1
OP-501	1
OP-502	1
OP-503	1
OP-72	1
OP-74	1
OP-75	1
Navy Department	
Washington, DC 20350	
Commander	
Space and Naval Warfare Systems Command	
Attn: SPAWAR-05	1
Washington, DC 20363-5100	

DISTRIBUTION (Cont.)

		Copies
Commander		
Naval Sea Systems Command		
Attn:	SEA-05R	1
	SEA-55	1
	SEA-55X	1
	SEA-55X1	1
	SEA-55X2	1
	SEA-55Y	1
	SEA-66U	1
	SEA-62	1
	SEA-62Y	1
	SEA-62Z	1
	SEA-63	1
	SEA-63D	1
	PMS-402	1
	PMS-406	1
	PMS-407	1
Washington, DC 20362-5105		
Commander		
Naval Air Systems Command		
Attn:	AIR-5004	1
	AIR-51623	1
	AIR-540	1
	AIR-5404	1
	AIR-93	1
	AIR-932F	1
	AIR-932H	1
	AIR-932K	1
	AIR-932T	1
	PMA-242	1
	Technical Library	1
Washington, DC 20361		
Commander		
Naval Surface Warfare Center		
Carderock Division		
Attn:	Technical Library	1
	Code 17	1
	Code 172	1
	Code 1740.3 (R. Garrison)	1
	Code 1740.4 (S. Wang)	1
	Code 175 (W. Sykes)	1
	Code 1750.2 (W. Conley)	1
	Code 1740.2 (F. Fisch)	1
Bethesda, MD 20084		

		Copies
Commander		
David Taylor Research Center		
Attn:	Code 177	1
	Technical Library	1
Portsmouth, VA 20375		
Commanding Officer		
Naval Research Laboratory		
Attn:	Technical Library	1
Washington, DC 20375		
Commanding Officer		
Naval Surface Warfare Center		
Dahlgren Division		
Coastal Systems Station		
Attn:	Technical Library	1
Panama City, FL 32407-5000		
Commander		
Naval Undersea Warfare Center		
Division		
Attn:	Technical Library	1
Newport, RI 02840		
Commander		
Naval Air Warfare Center		
Weapons Division		
Attn:	Code 3917	1
	Code 38 (R. Derr)	1
	Code 389 (T. Boggs)	1
	Code 32	1
	Code 3205	1
	Code 3208	1
	Code 326	1
	Code 3261	1
	Code 3263	1
	Code 3264	1
	Code 3265	1
	Code 3266	1
	Code 327	1
	Code 381	1
	Code 385	1
	Code 3850	1
	Code 3853	1
	Code 3891 (J.Covino)	1
	Code 39	1
	Technical Library	1
China Lake, CA 93555-6001		

DISTRIBUTION (Cont.)

	Copies
Commander Naval Surface Warfare Center Indian Head Division Attn: Code 2730D	1
Technical Library	1
J. Chang	1
P. Dendor	1
L. Newman	1
Indian Head, MD 20640-5000	
Commander Center for Naval Analyses Attn: Technical Library 2000 Suitland Road Washington, DC 20390-5140	1
Superintendent Naval Postgraduate School Attn: Library Monterey, CA 93940	1
President Naval War College Attn: Technical Library Newport, RI 02841	1
Commanding Officer Naval Amphibious Base, Coronado	
Attn: RDT Officer	1
SEAL Team	1
Underwater Demolition Team	1
San Diego, CA 92155	
Commanding Officer Naval Amphibious Base Little Creek	
Attn: RDT Officer	1
Norfolk, VA 23511	
Commanding Officer Naval Explosive Ordnance Disposal Technology Center	
Attn: Technical Library	1
Indian Head, MD 20640	

	Copies
Commander Pacific Missile Test Center Attn: Code 2145	1
Point Mugu, CA 93042	
Commanding Officer SEAL Team 2	
FPO New York, NY 09501-4633	1
Commanding Officer Naval Undersea Warfare Engineering Station	1
Keyport, WA 98345-0580	
Commanding Officer Naval SurfaceWarfare Center Port Hueneme Division	1
Port Hueneme, CA 93043-5007	
Commander Naval Weapons Evaluation Facility	
Kirtland Air Force Base	
Albuquerque, NM 87117	1
Commanding Officer Naval Surface Warfare Center Crane Division	
Attn: Code 3031 (E. Neal)	1
Code 50D (A. Norris)	1
Code 505 (J. E. Short)	1
Code 90 (A. E. Whitner)	1
Crane, IN 47522	
Commanding Officer Naval Weapons Station	
Attn: Code 321 (M. Bucher)	1
Concord, CA 94520-5000	
Commander in Charge Naval Surface Warfare Center Indian Head Division Yorktown Detachment	
Attn: Code 470A	1
Library	1
Yorktown, VA 23691-5000	

DISTRIBUTION (Cont.)

	Copies
Director Defense Nuclear Agency Attn: Technical Library Washington, DC 20305	1
Defense Science Board Attn: C. Fowler The Pentagon Washington, DC 20301	1
Director Defense Research and Engineering Attn: Library Washington, DC 20305	1
Director Defense Advanced Research Projects Agency Attn: Library 1400 Wilson Blvd. ARlington, VA 22209	1
Institute for Defense Analyses Attn: Technical Library 1801 N. Beauregard Street Alexandria, VA 22311	1
Commanding General Marine Corps Development and Education Command Attn: Library Marine Corps Landing Force Development Center Quantico, VA 22134	1
Army Armament Munitions and Chemical Command Attn: DRSAR-IRC DRSAR-LEM (R. Freeman) DRSAR-SF (R. Young) Rock Island, IL 61299-6000	1 1 1
Army Armament Research and Development Command Attn: Technical Library Dover, NJ 07801	1

	Copies
Redstone Arsenal Army Missile Command Attn: Chief, Documents D. Dreitzler Redstone Arsenal, AL 35809	1 1
Army Ballistic Research Laboratory Attn: SLC-BR-TB-EE SLCRBR-IB-I (P. Kaste) V. Boyle O. Blake G. Melani M. Chawla J. Trimble Technical Library Aberdeen Proving Ground Aberdeen, MD 21005-5066	1 1 1 1 1 1 1 1
Commander Officer Harry Diamond Laboratory Attn: Library 2800 Powder Mill Road Adelphi, MD 20783	1
Army Environmental Hygiene Agency Attn: HSHB-EA-A Aberdeen Proving Ground Aberdeen, MD 21005	1
Army Medical Bioengineering Research and Development Laboratory Attn: J. Barkeley Fort Dietrick, MD 21701	1
Commander Army Research Office Attn: G. R. Husk P. O. Box 12211 Research Triangle Park, NC 27709-2211	1
Army Toxic and Hazardous Materials Agency Attn: DRXTH-TE-D Aberdeen Proving Ground Aberdeen, MD 21005	1

DISTRIBUTION (Cont.)

	Copies
Commander	
Army Chemical Research, Development and Engineering Center	
Attn: SMCCR-DDP	1
Aberdeen Proving Ground, MD 21010-5423	
Wright Laboratory/Armament Directorate	
Attn: WL/MNME	1
WL/MNMW	1
WL/MNOI	1
WL/MNME (G. Glenn)	1
WL/MNMF (R.Mabrey)	1
WL/MNME (R. McKinney)	1
WL/MNMW (J. Foster)	1
Eglin Air Force Base, FL 32542-500	
Air Force Office of Scientific Research	
Attn: T. Matusko	1
Bolling Air Force Base	
Washington, DC 20332	
University of California	
Lawrence Livermore National Laboratory	
Attn: Technical Library	1
M. Finger	1
C. M. Tarver	1
J. D. Hallquist	1
L. M. Erickson	1
E. James	1
P. O. Box 808	
Livermore, CA 94550	
Los Alamos National Laboratory	
Attn: J. Repa	1
M. J. Urizar	1
S. W. Peterson	1
L. Smith	1
C. Forest	1
A. W. Campbell	1
R. Engelke	1
P. C. Crawford	1
Los Alamos, NM 87545	

	Copies
Sandia National Laboratories	
Attn: Technical Library	1
P. O. Box 969	
Livermore, CA 94550-0096	
Argonne National Laboratory	
Attention Records Control for:	
Richard Anderson	1
Technical Library	1
9700 South Cass Avenue	
Argonne, IL 60439	
The Johns Hopkins University Applied Physics Laboratory Chemical Propulsion Information Agency	
Attn: T. W. Christian	1
Johns Hopkins Road	
Laurel, MD 20707	
The Johns Hopkins University Applied Physics Laboratory	
Attn: Technical Library	1
Johns Hopkins Road	
Laurel, MD 20707	
New Mexico Institute of Mining Technology	
Attn: Code TERA (J. Joyner)	1
Technical Library	1
Socorro, NM 87801	
Applied Research Laboratory Pennsylvania State University	
Attn: Library	1
E. Lizka	1
P. O. Box 30	
University Park	
State College, PA 16801	
Defense Technical Information Center	
Cameron Station	
Alexandria, VA 22304-6142	12

DISTRIBUTION (Cont.)

	Copies
Royal Armament Research and Development Establishment	
Attn: Library	1
B. Hammant	1
Fort Halstead, Sevenoaks, Kent	
United Kingdom	
Materials Research Laboratory	
Attn: M. Chick	1
P. O. Box 50	
Ascot Vale, Victoria 3032	
Advanced Technology and Research, Inc.	
Attn: S. Jacobs	1
J. W. Watt	1
W. Pickler	1
Laurel Technology Center	
14900 Sweitzer Lane	
Laurel, MD 20707	
TRW	
Attn: R. Church	1
San Bernadino, CA 92401	
Aerojet Ordnance and Manufacturing Company	
Attn: G. Chin	1
9236 East Hall Road	
Downey, CA 90241	
Vanderbilt University	
Attn: A. Mellor	1
Nashville, TN 37235	
Lockheed Missiles and Space Company	
Attn: R. Hodges	1
J. Smith	1
P. O. Box 504	
Sunnyvale, CA 94086	
Hercules Incorporated Rocket Center	
Attn: G. Williams	1
P. O. Box 210	
Rocket Center, WV 26726	

	Copies
Hercules	
Attn: M. Klakken	1
M. Berger	1
L. Losee	1
T. Speed	1
Bacchus Works	
Magna, UT 84044-0098	
Thiokol Corporation	
Tactical Operations	
Attn: D. Jeff Jones, Materials and Process Development	1
Huntsville Division	
P. O. Box 400006	
Huntsville, AL 35815-1506	
Alliant Techsystems, Inc.	
Attn: K. L. Christianson	1
J. L. Houlton	1
G. Johnson	1
7225 Northland Drive	
Brooklyn Park, MN 55428	
Library of Congress	
Attn: Gift and Exchange Division	1
Washington, DC 20540	
Internal distribution:	
E231	2
E232	3
E342	1
G13 (D. L. Dickinson)	1
G13 (T. Wasmond)	1
G22 (W. H. Holt)	1
(W. Mock)	1
(S. S. Waggener)	1
R10	1
R101	1
R10 (R. R. Bernecker)	1
R10A (C. Dickinson)	1
R10B (H. S. Haiss)	1
R10A1	1
R10A2	1
R11	1

DISTRIBUTION (Cont.)

		Copies
R12		1
R12	(B. A. Baudler)	1
	(B. C. Glancy)	1
	(L. C. Hudson)	1
	(G. Laib)	1
	(L. L. Mensi)	1
	(L. J. Montesi)	1
	(P. F. Spahn)	1
	(T. Spivak)	1
R13		1
R13	(K. D. Ashwell)	1
	(R. N. Baker)	1
	(R. D. Bardo)	1
	(A. Brown)	1
	(C. S. Coffey)	1
	(J. Davis)	1
	(D. L. Demske)	1
	(J. W. Forbes)	5
	(R. H. Guirguis)	1
	(P. K. Gustavson)	1
	(R. N. Hay)	1
	(H. D. Jones)	1
	(K. Kim)	1
	(R. J. Lee)	5
R13	(W. W. Lee)	1
	(E. R. Lemar)	1
	(P. J. Miller)	1
	(C. T. Richmond)	1
	(H. W. Sandusky)	1
	(G. T. Sutherland)	1
	(D. G. Tasker)	5
	(W. H. Wilson)	1
	(D. L. Woody)	1
	(F. J. Zerilli)	1
R14		1
R14	(J. W. Koenig)	1
R15		1
R15	(S. Collignon)	1
R34		1
R34	(B. C. Beard)	5
R42	(R. Dewitt)	1
U10	(W. Wassmann)	1
U11	(R. Plenge)	1
	(D. Hinely)	1
U12	(C. Smith)	1
	(W. Hinckley)	1
U32	(G. Parrent)	1
U43	(L. Lipton)	

REPORT DOCUMENTATION PAGE

Form Approved
OMB No. 0704-0188

Public reporting burden for this collection of information is estimated to average 1 hour per response, including the time for reviewing instructions, searching existing data sources, gathering and maintaining the data needed, and completing and reviewing the collection of information. Send comments regarding this burden estimate or any other aspect of this collection of information, including suggestions for reducing this burden, to Washington Headquarters Services, Directorate for Information Operations and Reports, 1215 Jefferson Davis Highway, Suite 1204, Arlington, VA 22202-4302, and to the Office of Management and Budget, Paperwork Reduction Project (0704-0188), Washington, DC 20503.

1. AGENCY USE ONLY (Leave blank)	2. REPORT DATE	3. REPORT TYPE AND DATES COVERED
	May 1991	Final Report

4. TITLE AND SUBTITLE

Ignition of PBXW-115 Due to Electrostatic Discharge

5. FUNDING NUMBERS

Program Element No.
Project No.
Task No.
Work Unit No.

6. AUTHOR(S)

R. J. Lee, D. G. Tasker, J. W. Forbes, and B. C. Beard

7. PERFORMING ORGANIZATION NAME(S) AND ADDRESS(ES)

Naval Surface Warfare Center
10901 New Hampshire Avenue
Silver Spring, MD 20903-5000

8. PERFORMING ORGANIZATION REPORT NUMBER

NSWC TR 89-212

9. SPONSORING/MONITORING AGENCY NAME(S) AND ADDRESS(ES)

Office of Naval Technology
800 N. Quincy Street
Arlington, VA 22217-5000

10. SPONSORING/MONITORING AGENCY REPORT NUMBER

11. SUPPLEMENTARY NOTES

12a. DISTRIBUTION/AVAILABILITY STATEMENT

Approved for public release; distribution is unlimited.

12b. DISTRIBUTION CODE

13. ABSTRACT *(Maximum 200 words)*

Electrostatic discharge experiments were conducted on PBXW-115, an aluminized explosive. It was observed that this explosive conducts prior to catastrophic breakdown. However, these studies demonstrated that any significant reaction is confined to the discharge path following breakdown. *Sustained ignition* was not observed until the samples were restrained.

Shock energy fluence data for PBXW-115 were used to show that mechanical shock is the probable cause of ignition due to an electrical discharge. It was hypothesized that the thermal explosion of the material in the electrical discharge channel transmits a shock wave into the unreacted explosive. The explosive is subsequently ignited.

The analysis of the shock mechanics indicated that the degree of reaction caused by the electrical discharge is dependant on the diameter of the ignited channel. The channel diameters formed by electrical discharge in recovered explosive samples were found to be consistent with shock wave energy fluences necessary for *first reaction* according to this model.

14. SUBJECT TERMS			15. NUMBER OF PAGES
Electrostatic Discharge	Dielectric Breakdown	Mechanical Shockwave	60
Ignition	Arc Discharge	Energy Fluence	16. PRICE CODE
PBXW-115	Thermal Explosion		

17. SECURITY CLASSIFICATION OF REPORT	18. SECURITY CLASSIFICATION OF THIS PAGE	19. SECURITY CLASSIFICATION OF ABSTRACT	20. LIMITATION OF ABSTRACT
UNCLASSIFIED	UNCLASSIFIED	UNCLASSIFIED	SAR